ELECTRONIC TRANSPORT PROPERTIES OF SILICON NANOWIRES SYNTHESIZED BY LASER ABLATION

TAHIR ASLAN

A research report submitted to the Faculty of Science, University of the Witwatersrand, Johannesburg, in fulfillment of the requirements for the degree of Master of Science.

Johannesburg, 2015

DECLARATION

I declare that this research report is my own, unaided work. It is being submitted for the Degree of Master of Science in the University of the Witwatersrand, Johannesburg. It has not been submitted before for any degree or examination in any other University.

28th day of February 2015

ABSTRACT

In this thesis electron transport properties of silicon nanowires are studied. The devices are synthesized using a laser ablation technique. The catalysts used in the synthesis are nickel nanoparticles. The silicon nanowires are characterized by scanning electron microscopy, transmission electron microscopy, atomic force microscopy and Raman spectroscopy. Dielectrophoresis is used to align and contact nanowires across two electrodes to create two-terminal devices. In addition four-terminal devices are fabricated using PMMA lift-off based electron beam lithography. Electron transport properties of the fabricated devices have been studied using dc measurement techniques. Resistance of the silicon nanowires has been measured as a function of temperature and magnetic field. These measurements have been accomplished using a Cryogenics system at low temperature, and high magnetic field. Temperature dependent studies reveal that Arrhenius type thermally activated transport behavior is the dominant transport mechanism in measurements at zero magnetic field. Magnetic field dependent measurements show a weak positive linear magnetoresistance. There are also strong oscillations in magnetoresistance curves. The temperature and field independence of the oscillations has been attributed to quantum interference effects.

DEDICATION

To Muzeyyen Aslan and Ramazan Aslan

ACKNOWLEDGEMENT

I would like to express my heartfelt gratitude to Prof. Somnath Bhattacharrya, my supervisor, for giving me permission to undertake this research work and for his guidance on the progress of this work. I would also like to acknowledge the Head of School Prof. John Carter and Prof. Daniel Joubert for their help on administrative issues.

Special thanks to Mr Ali Ozturk for helping me in my relocation from Turkey to South Africa. He helped me with accommodation and paid fees for my master's studies. His moral guidance and encouragement is also highly appreciated.

The work discussed in this thesis went smoothly due to the help of my work colleagues. I would like to thank Dr. Davie Mtsuko for teaching me electron beam lithography and helping in the data analysis and proofreading of this document. I would like to acknowledge Dr. George Chimowa for his guidance in the high magnetic field and low temperature measurements. I would also like to acknowledge Chris Coleman and Siphephile Ncube for their support in the synthesis of silicon nanowires and TEM. I would also like to acknowledge Ross McIntosh for his help in scanning electron microscopy.

I am grateful to CSIR-NLC rental pool for the laser ablation facility established in our laboratory which helped me to produce my materials. The work reported in this thesis would not have been possible without Thomas du Plooy who set up the laser growth facility. Charles Sandrok is acknowledged for his help in the development of waveguides for device fabrication. I would also like to acknowledge Dr. Rudolph Erasmus for his help in Raman characterization of my material and Prof. Alexander Ziegler for giving me access to the Microscopy and Microanalysis facility. Special acknowledgement to Dr. Daniel Wamwangi for his help in RF sputtering for metallization of device electrodes.

I would like to thank my wife, Felek Aslan, for her support throughout my time as a masters student and for bearing with my absence when I attended to my studies. To help me cope through life as a graduate student I have been given parental support and encouragement by my parents Muzeyyen Aslan and Ramazan Aslan.

I would also like to thank my friends Fatih Yudulmaz, Suleyman Saglam, Abdullah Kaymakci, Imam Bakir Kaya, Emre Koca, and Huseyin Akdag for their friendship and encouragement during my studies.

The work discussed in this thesis would not have been possible without the financial support from the National Research Funding (NRF) and the Turkish Horizon Education Trust.

Table of Contents

LIST OF FIGURES

LIST OF TABLES

1 INTRODUCTION

1.1 Background and current research directions

The era of low dimensional silicon based materials can be traced back to the growth of silicon whiskers first reported in 1964 by Wagner and Ellis [1]. This was followed by the elucidation of growth mechanisms by Givargizov in 1975 [2]. A surge in the interest in research in silicon based nanomaterials was ignited when SiNWs with diameters < 20 nm and length > 1 μm were synthesized using a laser-ablation method by Lieber in 1998 [3]. Research on silicon nanowires devices was accelerated by the first report on a silicon nanowire field effect transistor device by Lieber in 2004 [4]. Since then there has been extensive investigations on the synthesis, properties, device fabrication and applications of silicon nanowires (SiNWs) [5]. The great interest in SiNWs is due to their unique properties which are remarkably different from bulk silicon. The novel electrical, optical and mechanical properties have attracted interest in nanodevice application and optoelectronics. There have been works on development of photonic applications based on the remarkable property of SiNW – the presence of a direct band gap – which makes them a good candidate for development of optically active materials [6].

There are therefore many experimental research works aimed at controlling of the bandgap for optoelectronic applications. A major research theme is on control of size and shape of the nanowires in order to make it possible for manipulation of properties like bandgap, effective mass and optical absorption [7]. Supporting these experimental approaches are theoretical works aimed at prediction of electronic properties of various silicon nanowires using numerical or computational tools such as density functional theory [8]. For example, Sacconi *et al*. used several models to define electronic properties of SiNWs such as Empirical Tight-Binding (ETB) model, the Linear Combination of Bulk Bands (LCBB) model and Non-Equilibrium Green Function (NEGF) model. They investigated the relation

between the diameter of SiNWs and the band gap of hydrogenated nanowires and found that when the diameter is 3.2 nm, the band gap is 1.56 eV. If the diameter is reduced down to 1.6 nm, the band gap increases up to 2.44 eV [9]. These theoretical works suggest that the bandgap is inversely related to the diameter and the way the nanowires surfaces are terminated affect the properties.

Silicon nanowires have also attracted the interest of low dimensional transport physics researchers. Many research works have been done on electronic transport properties of silicon nanowires at room temperature and low temperature. The room temperature works are important for device application since real important devices are operated at room temperature whereas the low temperature transport address fundamental physics questions on propagation of electrons in materials. Room temperature electronic transport studies on silicon nanowires include the work on high performance silicon nanowire field effect transistors (FETs) in which effects of thermal annealing and passivation on transconductance and carrier mobility were investigated [10]. Many other key FET parameters in silicon nanowires of the diameter range 10 to 20 nm and channel lengths in range 800 to 1000 nm have been studied. Another notable work was the work of Yi *et al.* on confinement induced quantum oscillations in transport which supported the theoretical predictions of enhanced mobility in strongly confined nanowire devices [12]. This work focused on sub-5 nm silicon nanowires.

There have also been some experimental studies on low temperature transport properties. Notable works in the low temperature regime include the work of Sellier *et al.*, on spectroscopy of a single dopant atom in silicon [13]. This study involved measurement of resonance tunneling conductance in the temperature range 0.1 K to 4.2 K. The electronic states were deduced from the resonances that appeared in low temperature conductance at energies below the conduction band edge [13]. There have been also some works in quantum oscillation features have been observed at low temperature. This includes the work that studied low dimensional subband effects in silicon quantum wire transistor made via electron beam

lithography and reactive ion etching [14]. The width of the quantum wire was 65 nm. Another similar but earlier work is that by Colinge *et al.*, which also observed oscillations in gate dependent transport characteristics [11]. Step-like and oscillation features were observed at temperature below 30 K.

Many groups have been looking at the optical and phonon related properties of silicon nanowires [15]. It was shown that aligned SiNWs could have superior phononic properties than a single SiNW [16].This work motivated us to explore the electronic and optoelectronic properties of silicon nanowire based devices. We shall look at the effect of magnetic field on SiNW based devices which has been lacking in literature.

We note that studies of magnetoresistance in silicon nanowires [17] have been rare unlike many works reported on nanowires of Ge [18] and GaAs [19]. However, anisotropic negative magnetoresistance has been observed in heavily phosphorous doped SiNWs [17]. The NMR was attributed to electron scattering by localized spins at phosphorous donor states. Druzhinin *et al*. explored magnetoresistance in large diameter Si, Ge and Si-Ge wires (20 μm) [20]. A large positive MR was observed in these nanowires. These works motivated us to study magnetoresistance of individual Si nanowires in details and establish the novel quantum features discussed below.

1.2 Aims and Objectives

There are three main aims of this study. First is to understand the charge carrier transport mechanism in silicon nanowire based devices and how various factors such as geometry, temperature, magnetic fields, signal frequency and the chemical structure affect the transport properties. As silicon nanowires are essentially one-dimensional (1D) devices, they also share some characteristics such as semiconductivity and quantum transport features with other one-dimensional structures like carbon nanotubes and narrow graphene nanoribbons, the results of our experimental work can bring new knowledge and add to what is already known in the physics of 1D systems where quantum mechanical phenomena are prevalent. Secondly, we

are interested in development of real world applications of nanowires with performance parameters that can beat the limits of performance of devices developed so far and reported in literature. The transport studies in this project will give us an insight into how we can control properties and improve performance. The third objective of this project is to enhance expertise in many techniques involved in the fabrication of nanoscale devices such as material synthesis, electron beam lithography, transmission electron microscopy (TEM), scanning electron microscopy (SEM), atomic force microscopy (AFM), Raman spectroscopy, high frequency measurements, high magnetic field measurement techniques and low temperature electrical measurements.

1.3 Motivation

Silicon has proven to be a very important material for development of electronic devices such as transistors, which are utilized in memory chips, and microprocessors for computers and portable electronic equipments. Miniaturization of the electronic devices is an ongoing endeavor in the fields of microelectronics and nanotechnology. My goal is to contribute to this effort by developing nanoscale electronic devices based on silicon nanowires which are one-dimensional structure with significantly different electronic properties compared to two- dimensional silicon electronic in conventional electronics. My experiments will include synthesis of materials and development of devices with an aim of improving quality of the materials and devices and then studying electrical properties with an aim of understanding the physics of materials and devices that could help in the development of methods to improve device performance. The devices I will make can find applications in high-speed RF electronics, high sensitivity chemical and biochemical sensors as well as memory devices. I will focus my study on magnetoresistance of nanowires and look for possibilities for how the devices can also be utilized in the future sensor technology.

1.4 Summary

This Thesis discusses the experimental work that was carried out to study electron transport properties of silicon nanowires.

Chapter 2 of this thesis presents the material silicon upon which silicon nanowires are based. A discussion of the electronic and mechanical properties of silicon nanowires is made. Theory of transport relevant to silicon nanowires and quantum wires in general is laid out.

In Chapter 3 the synthesis of nanowires is presented with emphasis on the technique and recipe of laser ablation of a bulk silicon target to produce silicon nanowires used in this work.

Chapter 4 constitutes the core work that was done in this project. The various characterization techniques including their working principles are discussed. Images of materials synthesized and nanowire devices fabricated as well as instruments used in this work are presented.

Chapter 5 presents our studies of various electronic transport properties including zero-field temperature dependence of resistance, current-voltage characteristics and magnetoresistance of silicon nanowires synthesized using a laser ablation technique. The origin of the oscillatory behavior in the magnetoresistance is also explained.

2 LITERATURE REVIEW

2.1 Semiconductor devices

Semiconductor devices are the foundation of the electronics industry. Semiconductor devices have been studied for over 125 years. There are about 18 major devices, and about 140 device variations related to them, which are the main building blocks of electronic gadgets. One of these building blocks is the metal-semiconductor junction in which there is a contact between a metal and a semiconductor. This device was the first semiconductor device ever studied in the 1874 [21]. The interface was used as a rectifying contact, that allows electrical current to flow easily only in one direction, or as Ohmic contact. It can also be used as the gate for a channel between two Ohmic source and drain terminals. The second block is the p-n junction diode which is a contact between a p-type (with positively charged carriers) and n-type (with negatively charged carrier) semiconductors. This is a key building block for most semiconductor devices and serves as the foundation of the physics of semiconductor devices. If another p-type semiconductor is added, a p-n-p bipolar transistor is created. The third block is the heterojunction interface which is an interface between two dissimilar semiconductors. One such heterostructure is made of gallium arsenide (GaAs) and aluminum arsenide (AlAs). The heterojunctions are important components for high-speed electronic and photonic devices. The fourth building block is the metal-oxide semiconductor (MOS) field effect transistor based on silicon. The MOSFET is an important device for advanced integrated circuit and the backbone of microelectronics industry.

In the field of microelectronics there has been a continued effort to miniaturize the devices in order to increase the number of devices per area of a microchip. This has promised to give large memory and improve performance of device. For example the cut-off frequency and the speed of

transistor devices have been increasing with reduction of channel length (See Fig. 2.1). Such efforts have led to device sizes down to 20 nm. In a similar pursuit of such nanoscale sized devices many structures and nanomaterials have been developed and studied. The structures include carbon nanotubes [27], conducting polymer nanowires [31, 32] and silicon and germanium nanowires [5, 12]. Recently they have also been lots of studies in graphene nanoribbons [33].

The main drive towards the study of these nanomaterials is their unique physical properties that are remarkably different from those of bulky materials due to quantum confinement. Earlier people worked on the phonon and quantum confinement of the SiNWs [15]. We can see these different properties in electronic transport, optics and magnetism.

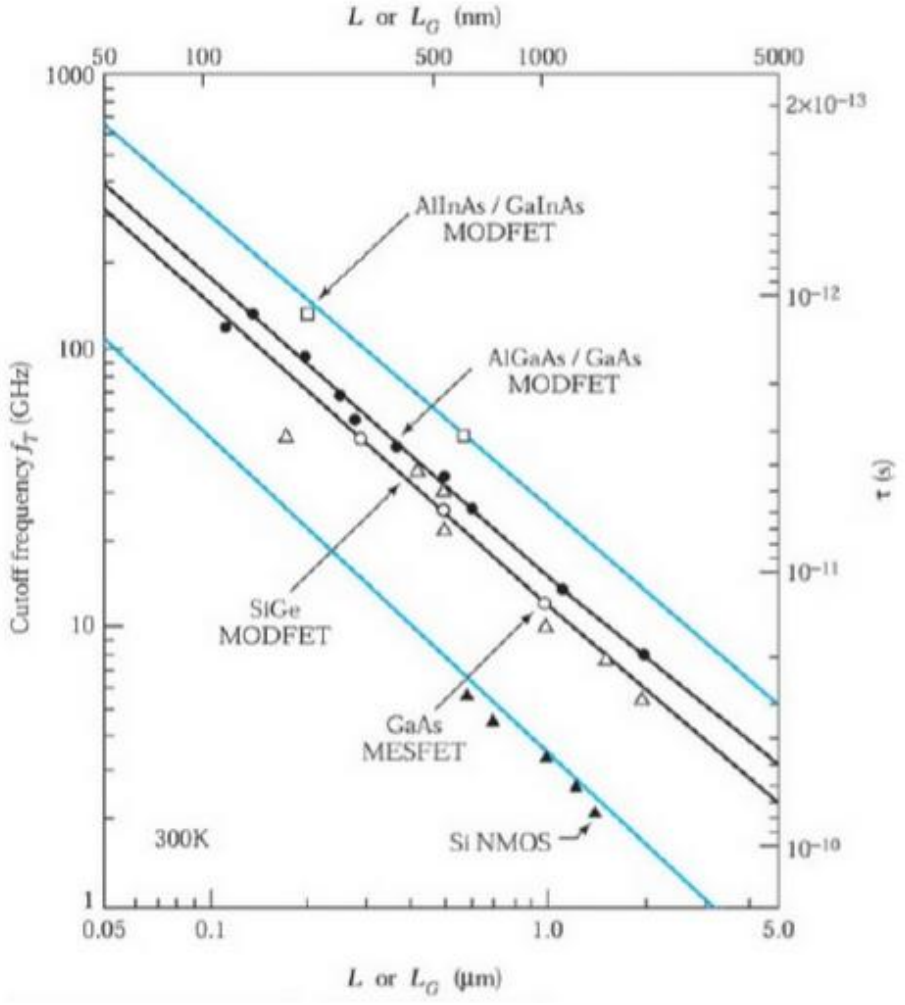

Figure 2.1: Cutoff frequency versus channel or gate length of five different field effect transistors [21].

2.2 Silicon

The group IV elements are C, Si, Ge, Sn, and Pb and their crystal structure is diamond cubic (Fig. 2.2 (a)). These types of material have identical electronegativities and the bond type is covalent.

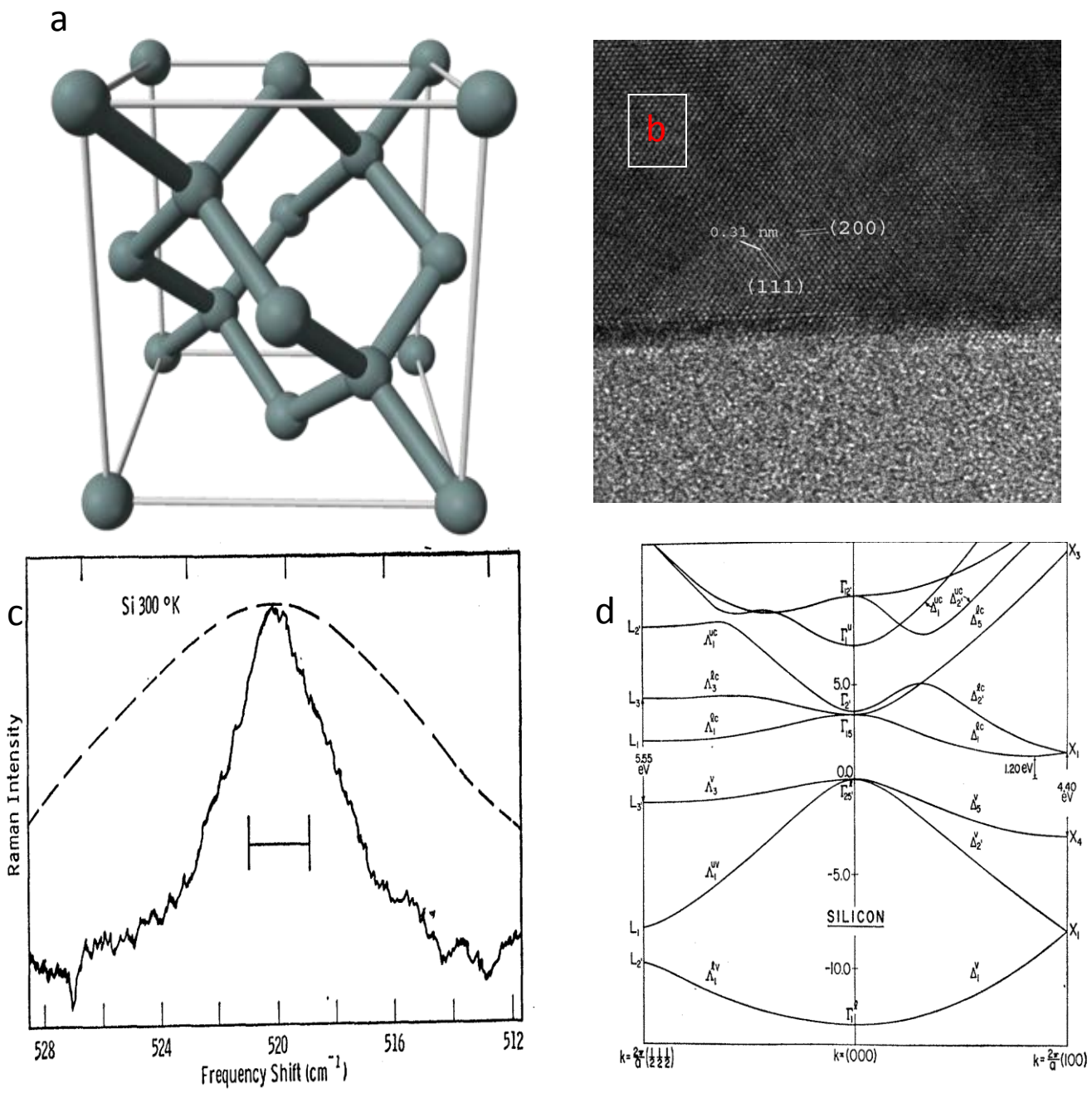

Figure 2.2: Structure of silicon. (a) Diamond cubic crystal structure. (b) TEM of single crystal Si [22]. (c) Raman spectrum of Si [23]. (d) Bandstructure of Si [24].

Silicon is a solid at room temperature. The atomic number of silicon is 14 and atomic weight is 28.085. Electron orbital configuration of Si is $1s^2 2s^2 2p^6$ [$3s^2 3p^2$] and from this we can see that the outer electron orbital is like carbon and also crystallizes like carbon in a diamond cubic crystal structure (See Fig 2.2 (a)). The lattice constant of silicon is 0.54 nm. The spacing between (111) crystal planes determined by X-Ray diffraction and TEM is about 0.31 nm (See Fig 2.2 (b)). Raman spectroscopy of silicon exhibits a very intense peak at 520 cm^{-1} (Fig 2.2 (c)). Silicon is also a reactive element and can form compounds such as SiO_2, Si_3N_4 and SiC. Intrinsic silicon is a semiconductor. As seen from Fig 2.2 (d) silicon is an indirect bandgap semiconductor [24]. Silicon can conduct electricity as well as heat. Silicon is a material on which the semiconductor industry is based. In this study, in the synthesis of silicon nanowires we used a silicon powder to make a laser ablation target or silicon source and used a silicon wafer (with a silicon oxide surface) as a substrate for dispersing the silicon nanowires and making devices.

2.3 Silicon nanowires

Diameter of synthesized nanowires can vary from several nanometers to about 100 nm. There are many different types of nanowires such as metallic (Ni, Pt, Au, etc.), semiconducting (Si, InP, GaN, etc.) and insulating nanowires (SiO_2, TiO_2, etc.). There are also organic molecular nanowires in which there occur repeating molecular that are electrically conductive such as the class of conjugated polymers [31]. We are interested in SiNWs. Fig. 2.3 shows a high resolution TEM image of a SiNW. We can identify both cubic and hexagonal phases in the SiNW, something which is different from single crystalline bulk silicon.

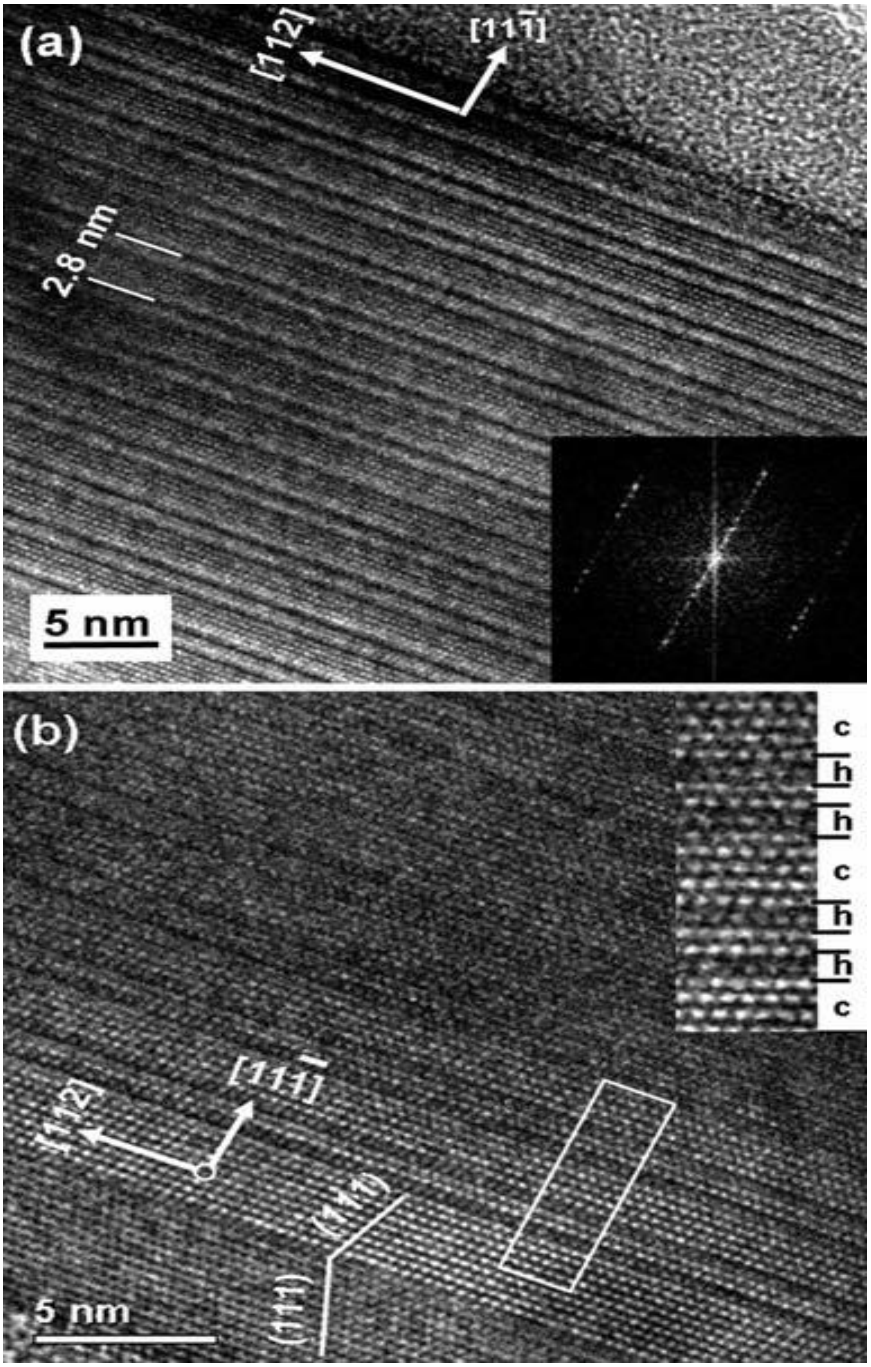

Figure 2.3: HRTEM image of a SiNW with regular intergrowth of the cubic and hexagonal phases. The inset is the corresponding FFT pattern. (b) Higher magnification HRTEM image of the surface area of the SiNW shown in (a) [25].

Semiconductor nanowires are generally synthesized using chemical vapor deposition (CVD) and laser ablation techniques. The synthesis is governed by a vapor-liquid-solid (VLS) growth mechanism [7,34]. The unique property of nanowires is their diameter that provide an opportunity for applications and realization of quantum transport features [34]. There are

many electronic transport studies on semiconductor nanowires (NWs) and nanowire based devices such as FETs [35, 36], inverters, photodetectors, nanosensors, light-emitting diodes, lasers, decoder, non-volatile memory and programmable logic. Intrinsic silicon is a large band gap semiconductor. Doping can reduce the bandgap. Doping of SiNWs to make n-type and p-type materials is crucial in making of practical nanoscale electronic devices and technology. One can fabricate p-n junctions, bipolar transistor and complementary inverters on SiNWs by selective doping of various regions of the nanowires [21]. One can characterize SiNWs as either n-type or p-type SiNWs by electronic transport measurement techniques. Research on nanowires began to accelerate in 1998, when SiNWs with diameters < 20 nm and length > 1 μm were synthesized using a laser-ablation method [3, 26]. Theoretical and experimental studies of transport reported in literature have mainly been on studied electronic properties of SiNWs such as the band gap, valley splitting and effective masses as functions of wire dimension [64].

In this research project, our primary goal is to synthesize high quality SiNWs by laser ablation method, and then characterize them using high resolution transmission electron microscopy (TEM), scanning electron microscopy (SEM), atomic force microscopy (AFM) and Raman spectroscopy. Secondly, we will fabricate two-, three- and four-terminal nanoscale devices using electron beam lithography and carry out systematic DC as well as high frequency measurements of electronic transport properties and magneto- resistance at room temperature and low temperature.

This research will help to clarify transport dynamics in nanoscale electronic devices and provide a catalog of performance parameters of nanoscale silicon electronic devices that will be a basis for new applications development and performance improvements in silicon based electronic devices.

2.3.1 Electronic Properties of silicon nanowires

Semiconductor nanowires have some unique properties such as quantum confinement effect, surface sensitivity and low leakage currents. Diameter, length, growth direction, chemical composition, and doping level of nanowires influence properties of the nanowires and devices made from these nanowires [7].

Silicon nanowires like any other type of nanowires are quantum wires in that they exhibit quantum confinement effects. In silicon nanowires quantum confinement affects the effective mass of carriers and the bandgap. The extent of the effect of quantum confinement depends on the surface termination of the nanowires. Theoretical studies done by Sacconi *et al.* have shown that effective mass change from $0.47m_e$ to $0.31m_e$ when silicon thickness is increased from 1.6 nm to 3.2 nm for H-terminated nanowires whereas in SiO_2 terminated SiNW the effective mass changes from $0.36m_e$ to $0.29m_e$ when the thickness of Si is increased from 1.6 nm to 3.2 nm [9]. In the same studies it was shown that reducing the size from 3.2 to 1.6 nm in hydrogenated nanowires increases the bandgap from 1.56 to 2.44 eV, whereas in SiO_2 terminated SiNW the gap increases from 1.50 to 1.88 eV.

Electronic properties are changed by addition of impurities or dopants. External elements such as boron and phosphorus can change the conductivity of SiNWs [10]. Addition of pentavalent impurities like phosphorous, arsenic and antimony yields n-type semiconducting nanowires in which electrons are the majority charge carriers whereas addition of boron (a trivalent impurity) leads to a p-type semiconductor in which holes are majority charge carriers. The dopant concentration can be determined by four-probe measurements. Usually, the dopant has to be substitutionally incorporated within the silicon lattice via ion implantation. The doping of Si nanowires can also occur due to metal catalysts during nanowires growth by laser ablation or CVD method using catalysts. The doping level determines

the density of states in the nanowires. Experimental studies by Vaurette *et al*. have measured density of states up to 10^{13} cm^{-2} for n-type and p-type doping level of 10^{20} cm^{-3} [37].

Dopant concentration also changes the mobility of Si bulk such that hole and electron mobility decrease as the impurity concentration increase because of ionized impurity atoms act as scattering centers for the charge carriers. It has been experimentally found that mobility increases from 95 to 250 cm^2/Vs as the phosphorous concentration is reduced in doped SiNW FETs [4]. The mobility of Si nanowires is determined by FET measurements in which the nanowires are placed on SiO_2/Si surface and the underlying silicon layer is used as a back gate for modulation of drain-source current. In these type of devices the surface of Si is usually passivated by a chemically stable oxide. A deposited oxide with low level charge at the interface is important for Si-based electronic devices and Si nanowires since the surface and interface properties can affect the electric characteristics of devices.

Electronic transport properties of silicon nanowire devices such as FETs are ultimately influenced by many factors such as quality of source-drain contact, channel length or gate length and gate oxide thickness. These factors affect device performance parameters such as ON-OFF currents, transconductance, subthreshold slopes and mobility. These parameters can be improved by thermal annealing of contacts and passivation of oxide defects. Thermal annealing and passivation have been shown to increase average transconductance from 45 to 800 nS and the average mobility from 30 to 560 $cm^2/V.s$ [10].

2.3.2 Mechanical property of SiNWs

The mechanical behaviors of semiconductor nanowires are difficult to determine due to the size. But, mechanical properties of semiconductor nanowires in device are important since the contact electrodes that supply

current to the nanowires change the temperature hence the nanowires are subject to expansion or when measurement is performed at low temperature, nanowires are subject to stress. The stress changes change its electrical conductivity because of they can generate dislocation inside the nanowire. The stress level in the nanowire, therefore, needs to be determined. From the stress measurements one can then determine the Young's modulus which is defined as the ratio of stress over strain.

Nanowires have small diameter. Hence, mechanical property characterization of nanowires is difficult to define. There are many research groups that used different methods and materials for measurement mechanical property of individual nanowires, most of them using an AFM based technique or home-build system incorporated within a TEM [34]. They used AFM technique in which a nanowire is deposited on a flat surface and scanned by tip of AFM (Fig. 2.4). There were wide range of mechanical properties which were determined by this method such as plastic deformation, Young's modulus, yield strength and force at failure [38]. Some experimental works found the values of Young's modulus for silicon nanowires to be 158, 186 and 210 GPa [39, 40, 41], a fracture strength of 12 GPa[42] and bending strength in range 0.3 to 17 GPa [39, 42].

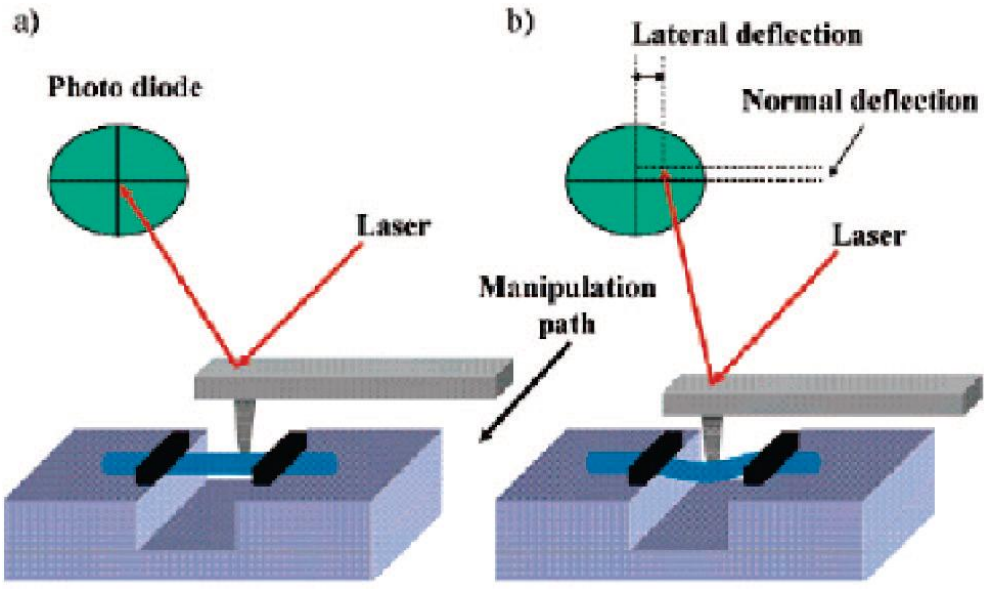

Figure 2.4: Experimental setup for measurement of mechanical properties of nanowires. (a) The tip approaches the wire and (b) the tip pushes the wire [38].

2.4 Theory of electron transport in silicon nanowires

Electronic properties of SiNWs depend on growth direction, morphology, size and surface functionalization. Diameter of SiNWs and band gap of SiNWs are in inverse relationship such as when the diameter decreases, the band gap increases and then deviates. Small diameter nanowires exhibit quantum confinement property. Other phenomena that can possibly be observed are negative differential resistance, linear magnetoresistance as well as conductance oscillation due to quantum interference. In this chapter the theoretical basis of transport in silicon nanowires is discussed.

2.4.1 Theory of transport in nanowires

Electronic transport of two-terminal silicon based devices can be described using various variables. One variable is conductivity, σ, which is the constant of proportional in the relation of current density, in the device channel and electric field applied across the device $j = \sigma E$. Of course one has to be careful in the use of conductivity when one deals with mesoscopic and nanoscale systems. Consider the case of bulk silicon system in which Ohm's law given by $V = IR$ is used. One can define a second Ohm's law given by $R = V/I$. One then makes use of ρ the inverse of conductivity to define $R = \rho A/L$. This last equation gives the impression that $R \rightarrow 0$ as L is reduced. However for nanoscale systems like silicon nanowires and carbon nanotubes R is a global quantity that cannot be decomposed into local resistivities. In this case one has to use the quantity $G = 1/R = I/V$ given in units of e^2/h as explained in next subsection. One has to treat a silicon nanowire as a one-dimensional (1D) quantum wire.

2.4.2 Conductance of 1D quantum wire

There are many approaches to calculate the conductance of quantum wires of which a silicon nanowire is one example.

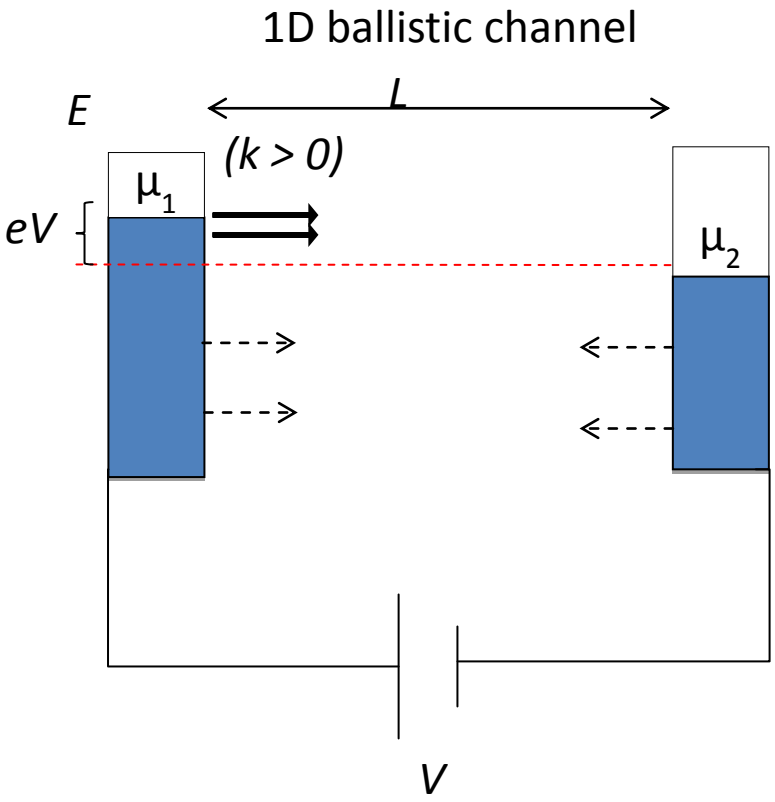

Figure 2.5: A one-dimensional ballistic transport channel.

If one considers contact to the nanowire as ideal reservoirs and define the chemical potential as $\mu \sim E_F$ where E_F is the Fermi level, and then considers transport without scattering, thus ballistic channel as shown in Fig. 2.5 one can define the current as given in equation 2.1

$$I = \int_{\mu_1}^{\mu_2} ev(E)\left(2\frac{1}{2}g_{1D}(E)\right)dE = \int_{\mu_1}^{\mu_2} ev(E)\left(\frac{2}{hv(E)}\right)dE = \frac{2e}{h}(\mu_2 - \mu_1) = \frac{2e}{h}(eV) \tag{2.1}$$

Where μ_1 and μ_2 are chemical potential for left and right leads, $v(E)$ is the electron velocity, h is the Planck's constant, e is the electron charge, V is the applied voltage, E is energy and the factor $\left(2\frac{1}{2}g_{1D}(E)\right)$ is the 1D density of states. The factors 2 are for spin degeneracy and number of modes with wavevector $k>0$. One then arrives at a result that the conductance can be given as

$$G = I/V = \frac{2e^2}{h} \tag{2.2}$$

This is fixed regardless of channel length *L*, and thus no well-defined conductivity. Another approach is to consider conductance from a point of view of transmission across a barrier. One makes use of the Landauer formula:

$$G = \frac{2e^2}{h}\Gamma \tag{2.3}$$

where Γ is the transmission probability. With N parallel 1D channel one can use the equation 2.4 valid at (T=0)

$$G(E_F) = \frac{2e^2}{h}\sum_n \Gamma_n(E_F) \tag{2.4}$$

This is equation is applicable at low temperature (T=0). At finite temperature one has to that electrons do populate the leads according to the Fermi-Dirac distribution:

$$f(E, E_F) = \frac{1}{\exp\left(\frac{E - E_F}{\kappa_B T}\right) + 1} \tag{2.5}$$

The conductance at finite temperature is thus given by equation 1.6 which can be observed as a smearing of conductance staircases.

$$G(E_F) = \frac{2e^2}{h}\sum_n \int \Gamma_n(E)\left(-\frac{df}{dE}\right)dE \approx \frac{2e^2}{h}\sum_n f(E_n - E_F) \tag{2.6}$$

For very high temperature the transport is incoherent due to dephasing due to inelastic scattering and phonons [43, 44].

2.4.3 Transport regimes

Transport in silicon nanowires is probed by microsized metallic leads which are electronically 3-dimensional compared to the one-dimensional nanowire channel. It is expected that the transimission probability across metal-semicondcutor junctions will be lowered due to symmetry mismatches for incoming and outgoing states at interfaces or presence of a Schottky barriers as is the case in semiconducting nanotube junctions [27]. If contact resistance is taken into account the resistance of the device is a sum of the intrinsic nanowire resistance (R_{nw}) and the contact resistance (R_c) given as: $R_{device} = R_C + R_{nw}$. The resistance of the nanowire depends on how the inter-electrode spacing of the device compares with some characteristic length scales determined by the nature of scattering processes encountered by charge carriers (electrons or holes) in the nanowire. In discussing transport in silicon nanowires the length scales to consider are the electron mean free path (l_e), localization length (L_0) and the phase coherence length L_ϕ. Localisation length is associated with elastic scattering on impurities without loss of phase, whereas the phase coherence length is associated with inelastic scattering that lead to phase decoherence. Depending on how the length of the nanowire compares with such characteristic length scales one can have coherent ballistic transport, diffusive transport, strong (Anderson) localization behavior and classical (incoherent) transport regimes. Typical scattering processes include electron-phonon scattering, electron-defect or impurity scattering. There can also be electron-electron interactions in the sample that can lead to Luttinger-liquid like behavior [46, 47].

2.4.3.1 Ballistic Regime

Ballistic transport refers to propagation of electrons without scattering in the nanowire. This occurs when the length of the nanowire is less than the localization length or phase coherence length. This means that there is no voltage drop along the nanowire and thus no resistance in the nanowire itself. However there is a voltage drop at the electrode-nanowire contact,

associated with a jump in the chemical potential difference between the nanowire and the electrodes, leading to a resistance given by the Landauer equation

$$G = \frac{4e^2}{h} \sum_i \int_{-\infty}^{\infty} \frac{df\left(E - E_F\right)/k_B T}{dE} \Gamma\left(E_F\right) dE \tag{2.7}$$

where $\Gamma\left(E_F\right)$ is the transmission probability of the *i*-th 1D subband at Fermi level and *f*(*E*) is the Fermi occupation function. For contacts with perfect transmission the expression reduces to

$$G = N \frac{2e^2}{h} \tag{2.8}$$

where *N* is the number of channels. In a single channel conductor *N*=1, R_Q ~ 13 kΩ is the inverse of the quantum conductance G_q. Ballistic transport has been experimentally observed in silicon nanowire field effect transistors of nanowire diameter 4 nm and channel length 22 to 408 nm [45].

2.4.3.2 Diffusive regime

When inelastic electron-phonon interaction becomes dominant phase coherence length of a nanowire becomes smaller than both the localization length and the length of the nanowire. Electrons propagate diffusively along the sample leading to Ohmic like transport behavior with resistance scaling linearly with length. In systems where diffusive transport is dominant conductance *G* can be expressed as

$$G = \frac{2e^2}{h} \frac{L_{ie}}{L} \tag{2.9}$$

where L_{ie} is the inelastic scattering length. At higher bias voltage there can be deviations from the Ohmic like behavior.

2.4.3.3 Strong localization regime

In unclean nanowires with large number of impurities and defects the electron wavefunction can be 'completely halted' or localized by the random potential of the defects and impurities. This is called the strong (or Anderson) localization regime. Transport of electrons in this regime is by means of tunneling processes, that is hopping conduction. The resistance of nanowires in such regime scales exponentially with length.

Considering these many possible regimes a discussion of transport need to provide information on the structural cleanliness of the samples, the measurement temperature and the bias voltage regime.

2.4.4 Thermally activated transport

As silicon nanowires are semiconductors it is natural to expect thermally activated transport. In the Arrhenius model the resistance of a material should scale as in equation (2.10)

$$R = \exp\left(E_g / 2k_B T\right) \tag{2.10}$$

Here E_g is the bandgap or the thermal activation energy. If there is some disorder in the system one can invoke the Mott's 3D variable range hopping (VRH) model or the Efros-Schlovskii (ES) 1D VRH for homogeneously disordered systems in which the conductance scales as in equation 2.11 in the insulating regime of the metal insulator transition

$$R = R_0 \exp\left[\left(\frac{T_0}{T}\right)^p\right] \tag{2.11}$$

where R_0 is a parameter that depends on the sample and the factor

$$T_0 = 4\pi/3N(\varepsilon_F)k_B L_0^3 \ , \tag{2.12}$$

where L_0 is the localization length and $N(\varepsilon_F)$ is the density of states at the Fermi level [31, 48]. The exponent P=1/(d+1)where d(=1,2 and 3) is the dimensionality of the hopping transport. In materials where electron-electron interactions are significant there is usually a cross-over from Mott 3D VRH to Efros-Schlovskii 1D VRH model where the temperature dependence of the resistance is

$$R = R_0 \exp\left[\left(\frac{T_{ES}}{T}\right)^{1/2}\right] \tag{2.13}$$

for all dimensions where T_{ES} is the characteristic ES temperature.

2.4.5 Magnetic field effects

Application of magnetic field is known to induce many effects on the transport of low dimensional systems depending on how the magnetic field is oriented with respect to the nanowire axis. A parallel magnetic field adds a Berry phase (Aharanov-Bohm phase) to a propagating electron wavefunction and can lead to opening up of gap in metallic nanowires such as carbon nanotubes. The AB effect can be measured experimentally as a fluctuation in conductance when plotted against magnetic field [49,50]. Such fluctuations are important probes for diffusive quantum transport in materials such as carbon nanotubes with typical signatures being weak localization and Altshuler-Aronov-Spivak oscillation for interference of a pair of time-reversed paths as well as universal conductance fluctuations for interference of different paths. In a weakly disordered system carrier electrons can scatter

off impurities and defects in different sequences, each with each trajectory having different phase. A magnetic field alters the relative phases of the carrier trajectories leading to random looking like but reproducible fluctuations in conductance δG of the order e^2/h. This is called universal conductance fluctuation (UCF). The magnetic field is able to do this because the phase acquired by propagating electrons depends on both the momentum (or wavelength) and the vector potential. Magnetic field can also induce splitting of spin-orbit degeneracy. Perpendicular field on the other hand can lead to formation of Landau levels which in the case of nanotubes are manifested as peaks in the vicinity of the charge neutrality point in density of states vs E plots [27]. The extent of magnetic field effects depends on the strength of the magnetic field and is usually more pronounced for high fields where magnetic lengths l_m are comparable to electron mean free path l_e. These magnetic effects which are best demonstrated in a nanotube which is an ideal one-dimensional system can also be observed in silicon and other semiconductor nanostructures [28, 29, 30].

2.4.5.1 Magnetoresistance

Magnetic effects are studied by measuring resistance as a function of magnetic field. Magnetoresistance is defined as $MR = \frac{R(B) - R(0)}{R(0)}$ where R(B) is resistance which change with field and R(0) is the resistance at zero field. Magnetoresistance of materials and devices is classified into ordinary magnetoresistance (OMR), giant magnetoresistance (GMR), colossal magnetoresistance (CMR), tunnel magneto resistance (TMR) and extraordinary EMR and Large magnetoresistance (LMR). To these we can add angular magnetoresistance (AMR) which describes magnetoresistance as a function orientation of field to the sample.

A generic quantum description of magnetoresitance was developed by Abrikosov [51]. In his description the quantum magnetoresistance is linear as given in equation 2.14.

$$\rho_{xx} = \rho_{yy} = \frac{N_i H}{\pi n^2 ec} \propto H\,, \tag{2.14}$$

where ρ_{xx} and ρ_{yy} are the transverse components of the magnetoresistance, N_i is the concentration of static scattering centers and n is the density of electrons [52].

This has been observed in bulky materials such as dichalcogenides, antimonides, rare earth metals, Si and Ge. The conditions for onset of linear magnetoresistance or for equation 2.15 to be valid are given in equation 2.15 [51].

$$n_0 << \left(\frac{eH}{\hbar e,}\right)^{3/2} \qquad T << \frac{eH\hbar}{m^* c} \tag{2.15}$$

In the mesoscopic scale linear magnetoresistance has been observed in transition metal nanowires. There also have been some reports on a non-quantum manifestation of linear magnetoresistance.

2.4.6 Silicon nanowire field effect transistors

Many transport measurements on silicon nanowire employ three terminal devices in which the effect of a gate voltage on device conductance can be studied (Fig. 2.6 (a) and (b)). In discussing silicon nanowire based field effect transistor one has to define the I_{ON}/I_{OFF} ratio which is the most significant parameter for characterizing performance of transistors. Mobility defined as a proportionality constant between the electron velocity and the electric field is another important parameter. The device conductance, current as well as the mobility will vary with gate voltage. The function of the gate voltage is to shift the Fermi level (E_F) with respect to the conduction band and valence band of the semiconducting silicon nanowire (Fig. 2.6 (d)). Thus one obtains higher conductance when the Fermi level is aligned with the valence band and conduction band edges. Alignment with the

valence band edge favours hole transport. This gives high current or conductance level on the left hand side of the zero gate voltage (or the OFF state). This state is referred to as the p-type ON state (See Fig. 2.6 (c)). If the Fermi level is aligned with the conduction band edge a conductance region is observed on the right hand side. This is referred to the n-type onstate. Whether the device is predominantly p-type depend on the doping of the nanowire. Many groups have developed field effect transistor devices [10, 63]. The field effect transport studies will be a focus of our future work.

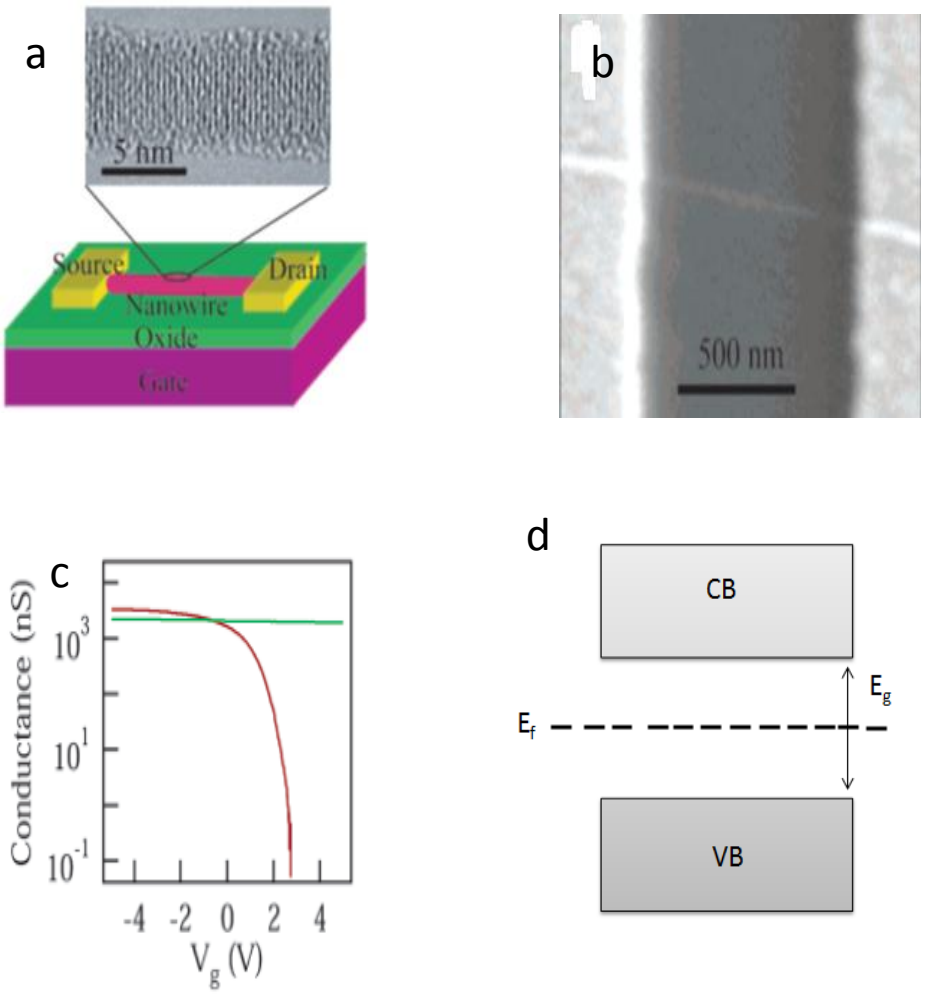

Figure 2.6: Schematic of a silicon nanowire FET device. (b) SEM image of the device. (c) Gate response of the SiNW FET device showing a p-type onstate. (d) A simplified band diagram of the FET device[10].

3 SYNTHESIS OF SiNWs

3.1 Introduction

Silicon nanowires (SiNWs) are attractive for both fundamental physics and application research. In this thesis we define SiNWs as an electrically conducting inorganic wires characterized by a small diameter (in the range 1 to 100 nm) and a long length which can vary from a few micrometers. The limit length is not known but will depend on the growth conditions.

There are two major paths to the development of silicon wires of such sizescale and high aspect ratio. One is a top-down technique accomplished by etching a block or bulk silicon layer progressively until the smallest possible width is reached. The second approach is the making of nanowires via bottom-up chemical synthesis techniques. The two approaches determine the research direction either towards industrial large scale integrated circuits applications or laboratory based fundamental research-oriented single device applications. The top-down approach makes use of a sequence of extreme UV photolithography or electron beam lithography and wet and dry etching steps that can selectively remove unmasked parts leaving the masked part intact which remains as final nanowire. This approach is a part of a standard approach used to develop semiconductor based electronic devices in industry and is part of a continued effort to miniaturize devices to improve performance of integrated circuits.

The second approach is synthesis of nanowires using vapor-liquid-solid techniques. This can lead to nanowires which are randomly oriented on a substrate. The nanowires can then be contacted with metal electrodes developed by electron beam lithography for single device fundamental research experiments. The random orientation prevent these from being applied in integrated circuits but they can find applications such as chemical and biological sensors [53, 54, 55].

3.2 Synthesis of SiNWs

SiNWs are usually grown via vapor-liquid-solid (VLS) method [5]. Semiconductor nanowires are generally synthesized using chemical vapor deposition (CVD) and laser ablation techniques. These are bottom-up nanowire preparation techniques. For this study, we used laser ablation method. There are four parameters for diameter control of SiNWs namely temperature, laser power, metal catalyst and gas flow rate during synthesis of nanowires. The diameter of SiNWs is an important factor for applications and realization of quantum transport features. Laser ablation can be used for synthesis of other types of NWs such as CdS, ZnS, GaN, p-GaN, Si-Ge or lnP. Vapor-liquid-solid method is generally used for growth of nanowires. Through this method and a metal catalyst (generally Au), Si and Ge nanowires can be grown by decomposing the source gas and forming a eutectic. In this method using disilane as the Si source, a higher degree of flexibility in tuning the stoichometry will be provided, and hence the bandgap can be controlled.

Apart from the synthesis techniques discussed above which are bottom-up techniques there are also top-down fabrication techniques for silicon nanowires which is accomplished by focused ion beam milling, photolithography, electron beam lithography and etching.

In this study, the purpose is synthesis of SiNWs and the study of electrical properties. SiNWs were synthesized by laser ablation method and contacted to electrodes using dielectrophoresis and electron beam lithography in order to investigate their electrical and magnetotransport properties. In this chapter we will give details about laser ablation and synthesis of SiNWs.

3.3 Synthesis of SiNWs by laser ablation

3.3.1 Laser ablation

In this study SiNWs are synthesized by pulsed laser ablation for characterization of electronic transport of 1D system. This section will explain laser ablation method and how the SiNWs were synthesized by laser ablation. The principles of working of a laser are beyond the scope of this work [56, 57]. When a laser pulse is incident onto the surface, it removes small particles of material. Similarly, when high-energy laser beam is incident onto silicon target, material is removing from the surface. Fig. 3.1 is a schematic of synthesis by laser ablation. Section 3.3.4 will give more information about synthesis of nanowires.

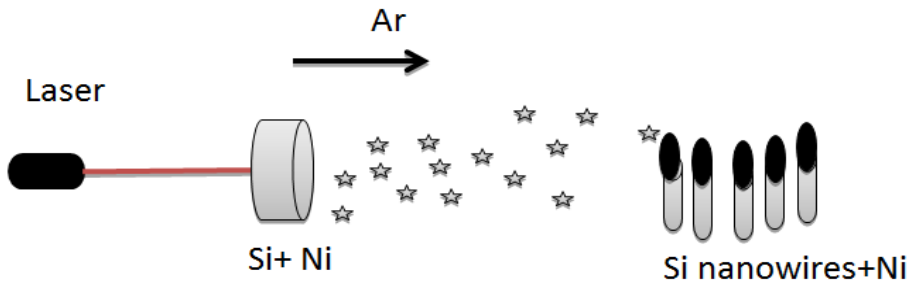

Figure 3.1: Illustration of laser ablation.

3.3.2 Nd: YAG laser

An Nd: YAG laser source was used for ablation. Nd:YAG is an acronym for the material Neodymium: Yttrium- Aluminum- Garnet ($Y_3Al_5G_{12}$). Nd:YAG is triangular crystal that is used for shifting laser radiation. The fundamental parts of the laser source are power supply, cooling system, resonator and analog controller. The power supply is used for producing a beam of laser to the resonator. A cooling system is fitted to the laser source

to prevent interruption of the laser (a chiller is supplied for cooling). The resonator is opposite two mirrors one of which is used for reflection of the beam whilst the other one is used for transitioning of the laser beam. An analog controller provides local beam control. Beam positioning is controlled by a LabVIEW software program.

In this study the Quanta-Ray series Nd:YAG laser was used. It has 1064 nm wavelength. The source is frequency doubled to yield 532 nm at 10 Hz. Pulse duration is 10 ns. It also has two mirrors, an aperture and a lens outside of laser source for orientation of the laser beam, adjustment of the beam size and determination of the target position respectively.

3.3.3 Beam alignment

Firstly the target is placed in the synthesis chamber and the following steps for alignment of beam are executed:

1. Turn chiller on.
2. Turn nitrogen purge on around 5.5 on the needle valve of the cylinder.
3. Turn laser power source on.
4. Allow 20 minutes for laser coils to warm up.
5. Switch laser in the long pulse mode to low energy oscillation 2.
6. Locate the beam position using ZAP-IT laser alignment paper.
7. Use first mirror for adjusting in the x- and y- direction.
8. Use aperture is for adjusting the size of the beam.
9. Use the second mirror for adjusting beam position (it can be adjusted manually and through LabVIEW program).

3.3.4 Recipe for Synthesis of SiNWs

The target is an alloy of silicon and metal catalyst. In this study nickel used for metal catalyst. The target is prepared by first mixing silicon (99%) and nickel (1 %) powder and then the powders are mixed with a binder that it is

polyvinyl alcohol dissolved in ethanol. The composite is then put into a steel mould of diameter 15 mm and pressed at 5.5 tonnes for 10 min to make a

pellet. The pellet is removed under the mould by inverting the main mould and pressing gently to remove the target. Finally, the pellet is placed in an evacuated tube which is placed in an oven. The oven temperature is increased stepwise in steps of 100 K from room temperature (300 K) to 1150 K in argon flow. Argon flow removes the binder and unknown impurities. There are two important things to bear in mind as a precaution - one is thermal shock and the other one is material oxidation. Therefore the temperature is decreased stepwise and argon flow is used during cool down until reaching 300 K. The target diameter is 15 mm and the length dependent on the amount of power. It is kept in a dry and clean place for purity. The target is ready for ablation. The target properties are too important for quality of SiNWs.

After preparing the solid target, it is ablated by laser. NWs have been synthesized by ablating solid targets with different compositional profiles by a Quanta-Ray PRO-270 Pulsed Nd: YAG laser. The process parameters such as temperature of synthesis, gas flow, target position, pulse energy, pulse duration, frequency, pulse energy, beam focus, chamber pressure are given Table 3.1.

Process parameter	**Specific values for synthesis SiNWs**
Target composition	99%Si, 1%Ni
Pressure	550 mbar
Temperature	1150 K
Gas flow rate	50 sccm
Flow tube inner diameter	25 mm
Beam spot size	3 mm
Frequency	10 Hz
Pulse duration	10 ns
Pulse energy	520 mJ

Table 3.1: Process parameters for synthesis of SiNWs.

The ablation process occurs in a sealed quartz tube placed in a furnace. The target was placed centered in a quartz tube with an inner diameter of 25 mm that was passed through a 1.2 m tube furnace. The laser was programmed to ablate sequentially. The furnace temperature in operation was stable between 873 and 1373 K. To produce the as-prepared material containing significant amounts of 1D nanomaterials, the laser was allowed to raster the target surface for about 1 hr by means of motion controlled steering mirrors. These mirrors are positioned just before the entrance of the quartz tube. After each run the system was allowed to cool down and the material for sample characterization was scrapped on the inside back-end of the quartz tube. Si containing 3%wt nickel target was ablated at a temperature of 1150 ^{o}C, pressure of 550 mbar and Ar flow rate of 50 sccm to produce SiNWs. Similar synthesis parameters have been reported in literature [58]. The laser setup is illustrated in Fig. 3.2.

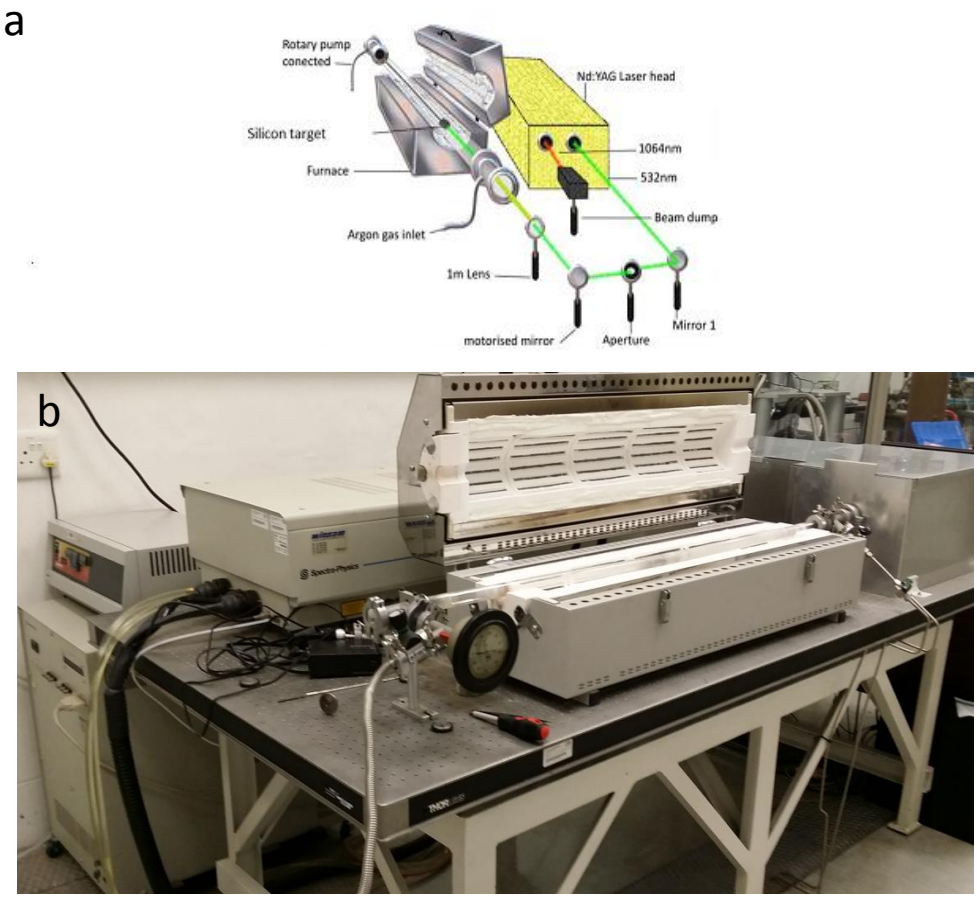

Figure 3.2: Laser setup for synthesis of SiNWs. (a) Schematic image of laser ablation of synthesis. (b) The laser ablation set up used in this work.

In this system, laser energy and temperature are used to ablate material. Gas flow is used carry plume, which is including silicon atoms and nickel particles. The particles are moved from a hot zone to the cold region. SiNWs grows and form in the cold region on the walls of flow tube. Finally, SiNWs were put in ethanol, which is used as a solvent, and sonicated by an ultra-sonicator.

3.4 Summary

Laser ablation was described and the recipe for synthesis is also discussed. We used laser ablation method for synthesis of SiNWs for this study. This method supported variety of opportunity easily during synthesis such as we can adjust size or diameter of material by temperature, laser power, and gas flow. Control of diameter is important for the control of electronic property of material for example bandgap which is inversely related to diameter.

4 EXPERIMENTAL METHODS

4.1 Introduction

In the previous chapter (3) we discussed the synthesis of the SiNWs. In this chapter we focus on the experimental techniques employed in the characterization of the SiNWs. We provide in much detail the device fabrication methods and how the electronic transport properties are studied. In particular, we investigate the 1D electrical behavior of SiNWs in order to understand their electronics properties. The SiNWs are aligned across two electrodes (drain and source) in a two-terminal device configuration. Other devices were contacted in a four-probe (four-wire sensing) measurement geometry.

4.2 Characterization

4.2.1 Introduction

SiNWs have to be properly characterized before their use in development of electronic devices and before any electrical measurement. The characterization techniques used in this work include Raman spectroscopy, scanning electron microscopy (SEM), transmission electron microscopy (TEM), atomic force microscopy (AFM).

4.2.2 Raman spectroscopy

The laser is a fundamental part of Raman spectroscopy. The other components of Raman spectroscopy include light collection optics, selector and a charge-coupled device (CCD). Here we use Raman spectroscopy as a tool for characterization of silicon nanowires. In the next subsection the principles of Raman spectroscopy are discussed.

4.2.2.1 Principles of Raman spectroscopy

A molecule consists of atoms. The atom consists of a nucleus and electrons which are different from each other. This property of atoms gives the identity of atoms and is also fundamental to Raman spectroscopy. When light is incident on a molecule, the light scatter from the molecule. This is demonstrated by Fig. 4.1.

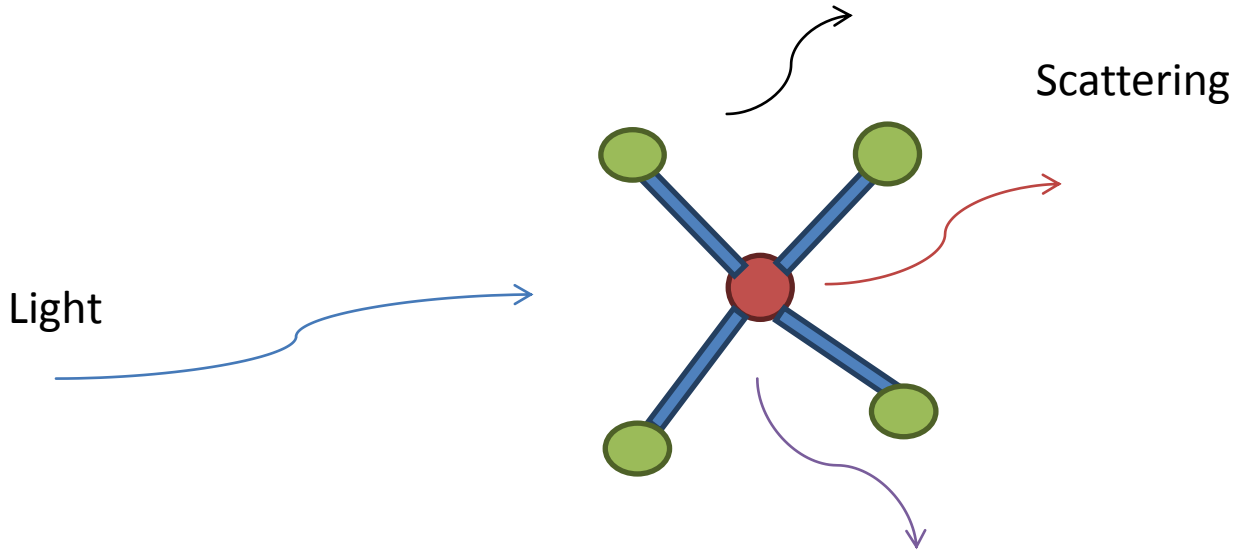

Figure 4.1: A beam of laser scattered by a molecule.

This scattering is the basis of Raman spectroscopy effect. Raman spectroscopy is the measurement of wavelength of scattering light and their intensity from molecules. When photon is interacting with molecule with frequency (υ_0), the photon changes frequency (υ_m) and energy because the energy of the photon is absorbed by molecule during the scattering. This scattering is inelastic or Raman scattering. If the photon loses energy the scattering is referred to as Stokes scattering and if the photon gains energy the scattering is referred to as anti-Stokes scattering. Fig. 4.2 demonstrates Stokes and anti-Stokes scattering.

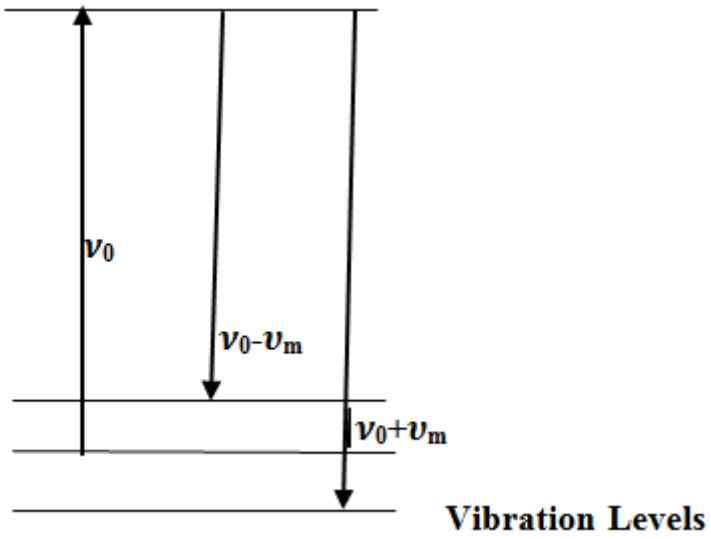

Figure 4.2: The energy level diagram for Raman scattering: Stokes (ν_0-υ_m) and anti- Stokes (ν_0+υ_m) scattering.

4.2.2.2 Characterization of SiNWs by Raman spectroscopy

A LabRam HR Raman spectroscopy instrument (Fig. 4.3 (a)) was calibrated by a silicon wafer. The characterization was done under room temperature and ambient pressure. SiNWs were dispersed on a glass substrate holder and analyzed by Raman spectroscopy. Laser wavelength of the beam, which is main part of Raman spectroscopy, was 514 nm (green) and power was adjusted to about 1.5 mW. This laser power is sufficient for the sample as well as the high spot integration time. If this value is too high, the sample can be damaged. The laser power should be between 1-10 mW.

The material was ultra-sonicated for 5 minutes in ethanol using a Heilscher UP400S sonicator. A small droplet of SiNW materials was dispersed on the glass surface and allowed to dry before characterization. In this way there is no thin film of SiNWs which can give different spectra.

Fig. 4.3 (b) shows Raman spectra of a silicon nanowire used to fabricate a device (sample B) and bulk silicon. The Raman shift of 520 cm^{-1} is observed for both bulk silicon and SiNW. This shows that the nanowires grown are

really made of silicon. The broad peak is comprised of a small SiNW peak obscured by a broad silicon oxide peak.

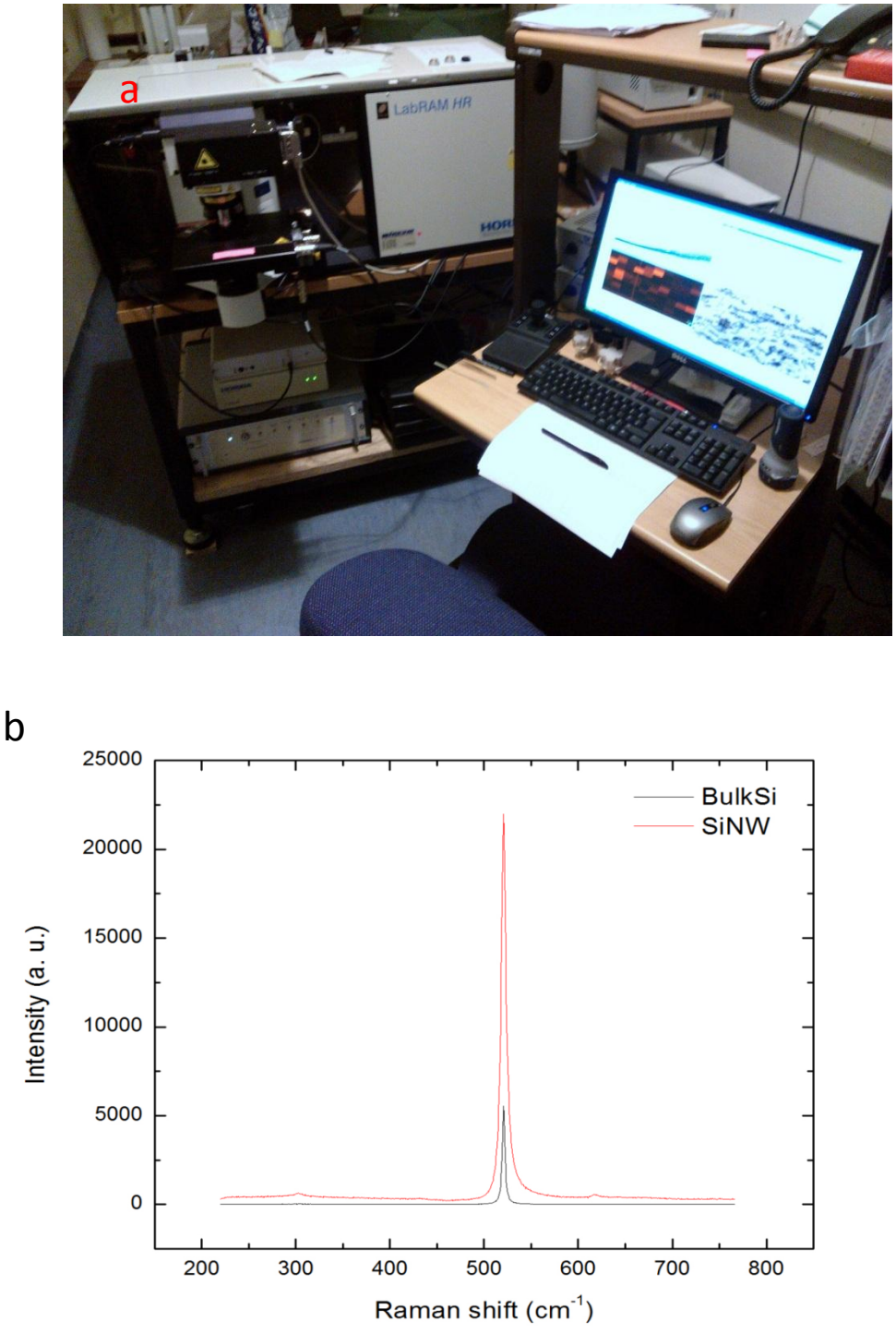

Figure 4.3: (a) A Raman spectroscopy instrument used for characterization of nanowires. (b) Raman spectra of a silicon nanowire used in fabricating device B. The black curve is for bulk silicon.

4.2.3 Scanning electron microscopy

4.2.3.1 Introduction

The principle of scanning electron microscopy (SEM) is based on electrons. Therefore the properties of electrons are important in the description of an SEM instrument.

Resolution of SEM is between that of light microscopy and transmission electron microscopy (TEM). This means that the SEM provides image resolution better than light microscopy and worse than TEM. The resolution of the SEM is sufficient to image silicon nanowires. In this section we describe the basic principle of a SEM, applications of SEM, and how it was used to check for the presence of nanowires and surface morphological analysis.

4.2.3.2 Electron

Electrons have a negative charge and when a negatively charged particle moves around, it produces magnetic field. This result in an electromagnetic field such that the electron behaves like electromagnetic wave which have wavelength, magnetic field and electric field. The electron wave like behavior is illustrated in Fig. 4.4.

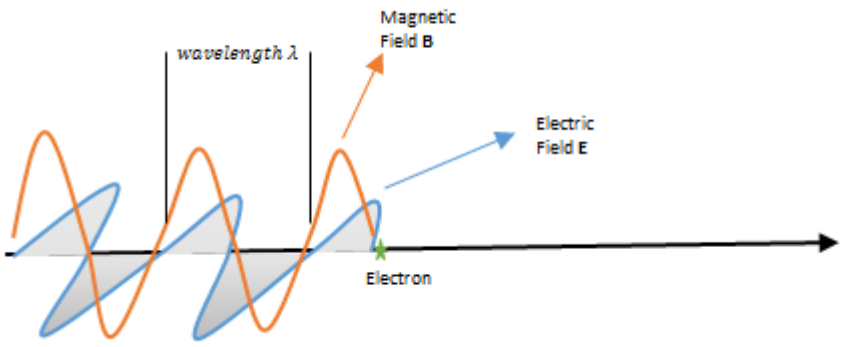

Figure 4.4: The wave-like behavior of electron.

This property of electrons means that we can orient electrons and we can focus an electron beam by both electric field and magnetic field. This property is important for science and applications of scanning electron microscopy. This property of electron is shown in Fig. 4.5.

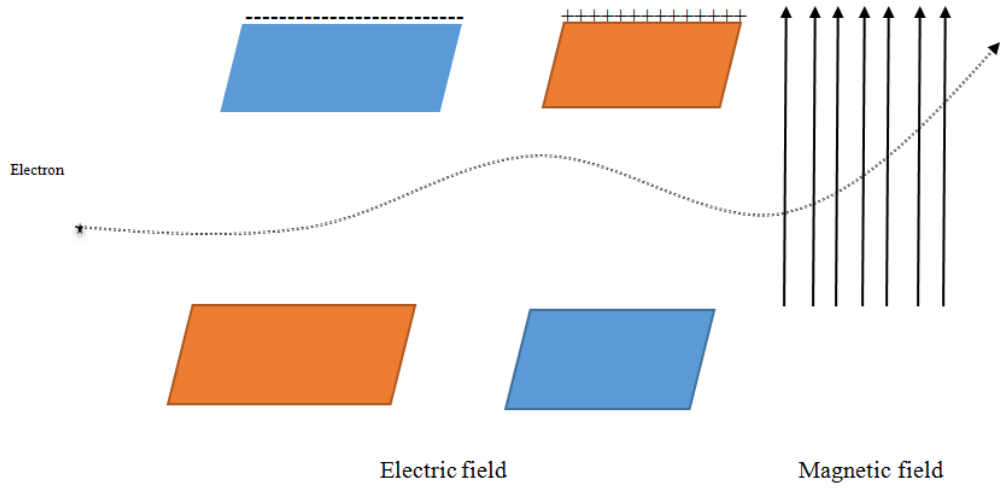

Figure 4.5: The behavior of electron in an electric and a magnetic field.

The other property of accelerated electrons is reflection. The electrons can be reflected from a material and due to their kinetic energy the electrons can ablate electrons from inside of a surface such as in photoelectric effect. Otherwise, if the accelerated electrons enter a solid surface, they scatter elastically and inelastically resulting in the formation of image. The electron can interact with atomic nuclei and atomic electrons. Inelastically interaction yields extra electrons and this is disadvantageous in the focusing image and can deform the specimen. Here electron acceleration voltage and incident angle is important. In the next subsection the main parts of a scanning electron microscopy are discussed.

4.2.3.3 Principle of scanning electron microscopy

There are different kinds of electron sources in the SEM such as tungsten filament, LaB_6, tungsten field-emission tip, etc. These sources generally supply maximum acceleration voltage of 30 kV. There are some lenses used

to orient the electron beam for formation image namely the condenser lenses and the objective lens that forms small probe. Electron probe incident beam has a small diameter. This probe can be scanned x and y direction. X direction scan is faster than y direction scan and are generated respectively by a sawtooth-wave and second sawtooth-wave generator. These generators are applied to a display device which show SEM image. Fig. 4.6 (a) shows the schematic diagram of SEM [59].

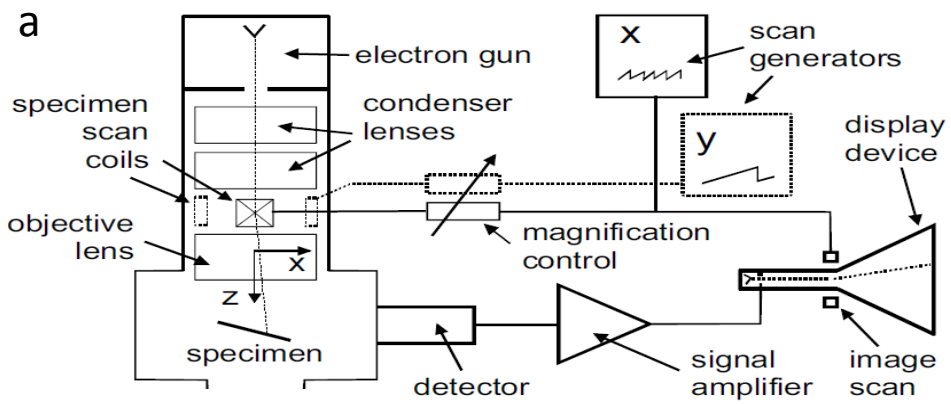

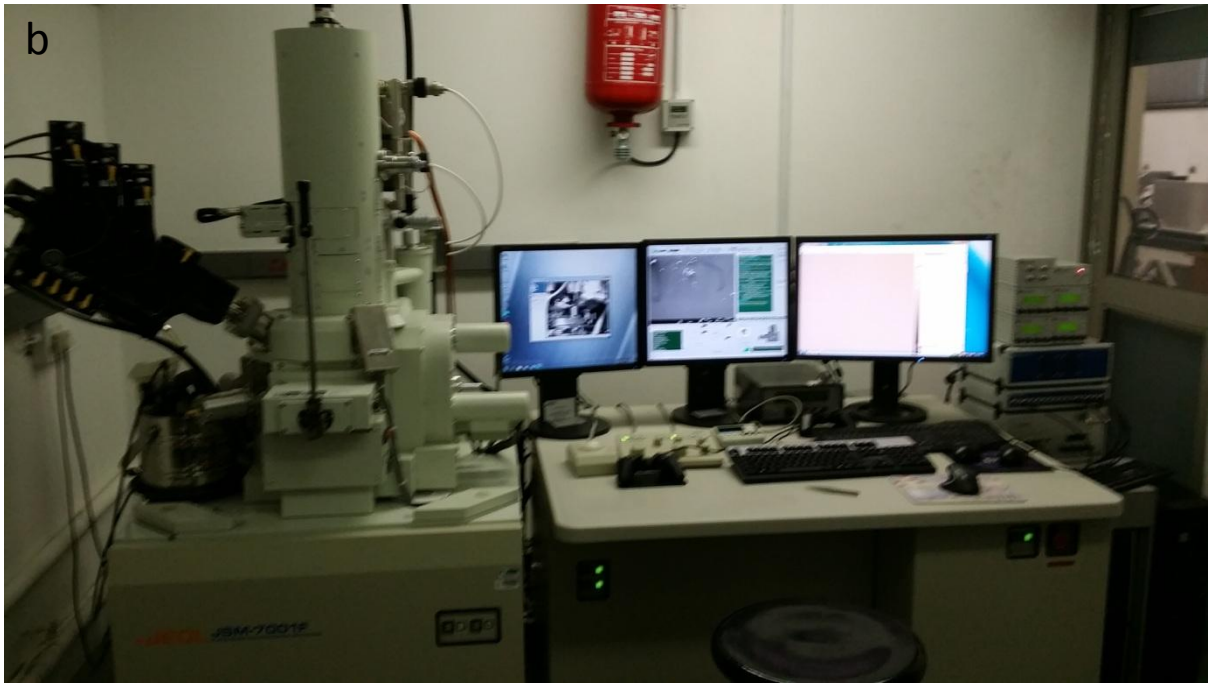

Figure 4.6: (a) Schematic diagram of a scanning electron microscopy [59]. (b) Picture of the SEM instrument used in this work.

4.2.3.4 Characterization of SiNWs by SEM

In this work we used a JEOL 7001-F scanning electron microscopy (SEM) to look for nanowires and study their surface morphology (See Fig. 4.6 (b)). This kind of SEM has acceleration voltage in the range 1 kV to 30 kV. The magnification is in the range 25 times to 1200000 times and operating vacuum is 10^{-8} Pa for high resolution image.

Kleindek Nanomanipulators and Omni-GIS are coupled to the microscope which are used respectively change the position of nanowires and remove undesired particles and contacting nanowires to electrodes. The SiNWs are sonicated for 12 h in ethanol solvent for dispersion of nanowires and deposited on the silicon (SiO_2/Si) wafer or glass substrate then allowed to dry. The wafer is then mounted on the stage of SEM by carbon tape which is also used to minimize charging effects. SiNWs are visible at acceleration voltage of 3 kV, spot size of 3 mm and in high vacuum (9×10^{-5} Pa). The SiNWs image obtained by SEM is shown in the next chapter.

Fig. 4.7 (a) and (b) show SEM images revealing the morphology of SiNWs dispersed on a glass substrate. The small white particles more apparent in the figures are Ni catalyst particles.

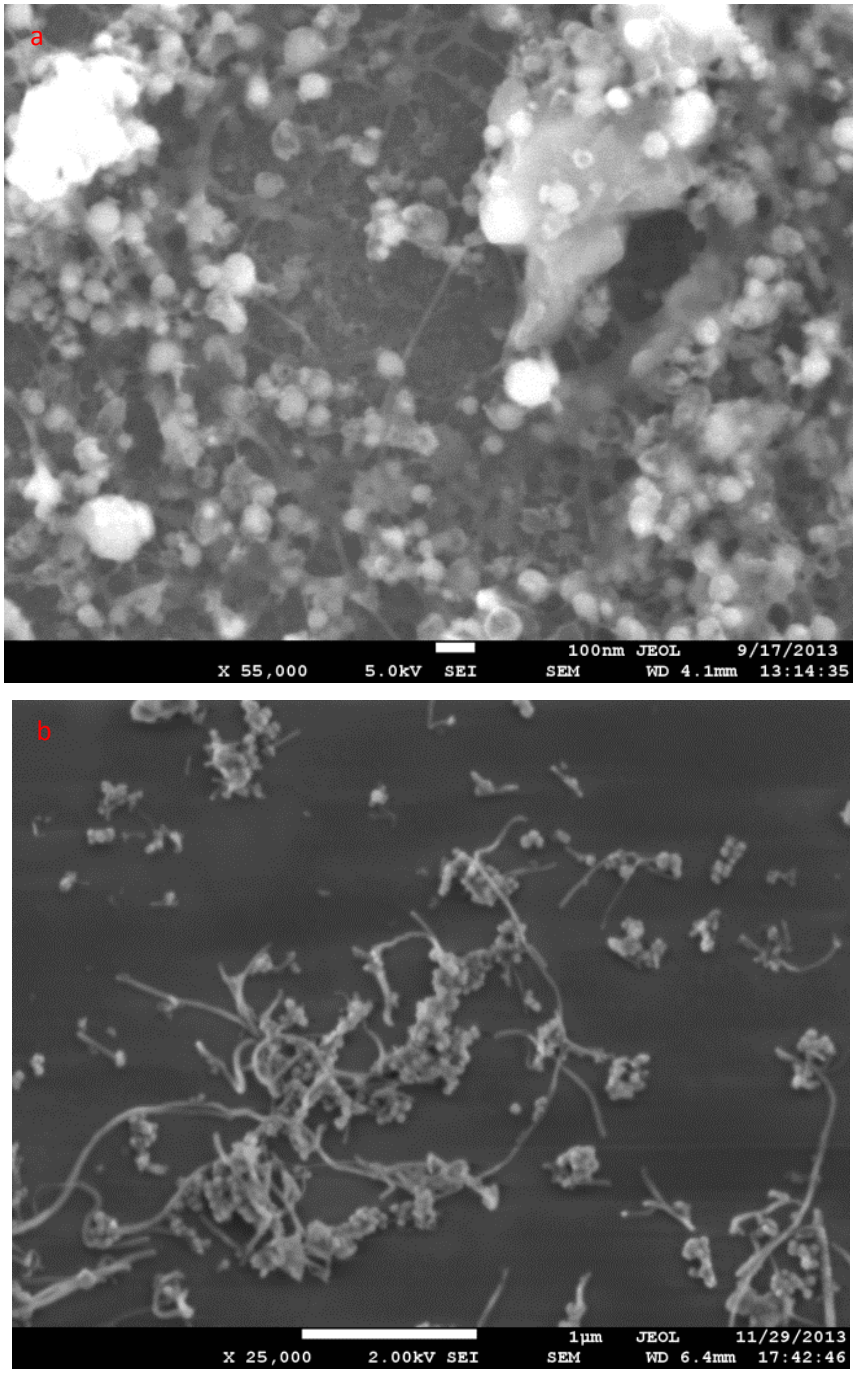

Figure 4.7: (a) SEM image of a mixture of silicon nanowires and nickel catalysts particles after synthesis. Scale bar 100 nm. Image of nanowires after dispersing in ethanol.

4.2.4 Transmission electron microscopy

4.2.4.1 Introduction

Fundamental basis of transmission electron microscopy (TEM) is also electrons like SEM which we explained above. Most of TEMs have electron acceleration voltage in the range 100 kV and 300 kV. The next subsection discusses the basic principle of a TEM, applications of TEM and also how it was used to take high resolution images of silicon nanowires and study their surface morphology.

4.2.4.2 Principle of TEM

Principle of TEM is based on electrons as explained above. The first TEM was built by Max Knoll and Ernst Ruska in 1931. This group developed the first TEM with resolution greater than that of light microscope in 1933 and thereafter a first commercial TEM in 1939.

TEM has resolution better optical lithography owing to the small de Broglie wavelength of electrons. The TEM has also resolution better than SEM. This enables the user of the instrument to examine fine detail. With TEM one can see even as small as a single column of atoms. This is thousands of times smaller than the smallest resolvable object in a light microscope. TEM is a major analysis method in a many scientific fields especially physical and biological sciences. TEMs find application in virology, cancer research, materials science, semiconductor research and nanotechnology.

At smaller magnifications TEM image contrast is due to absorption of electrons in the material due to composition and thickness of material. At higher magnifications complex wave interactions modulate the intensity of the image, requiring expert analysis of observed images. Alternate modes of use allow for the TEM user to observe modulations in crystal orientation, chemical identity, electronic structure and sample induced electron phase shift as well as the regular absorption based imaging.

The TEM is used in imaging of thin specimens. Electron gun is electron source that produce the electrons for TEM which are transmitted through the thin specimen. Electron gun consist of a filament which is made by tungsten (W) wire and connected to a DC current source that heat the filament to emit electrons. The electrons are focused by some lenses and transmitted through the specimen. The transmitted electrons are reflected on the fluorescent screen, a photographic film or captured by a CCD camera for observation of image Fig. 4.8 shows a schematic diagram of TEM

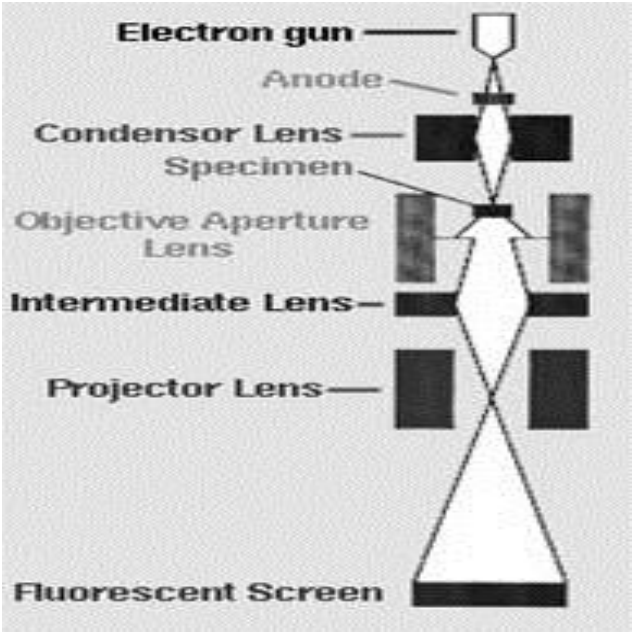

Figure 4.8: Schematic diagram for TEM.

4.2.4.3 Characterization of SiNWs by TEM

The FEI Spirit Transmission Electron Microscope (TEM) was used for structural analysis of SiNWs in this study. The microscope operates at a transmission voltage of 120 kV and standard magnification of 10^6 times. The SiNWs are sonicated for 12 h in ethanol solvent for dispersion of nanowires and then deposited on a copper grid then allowed to dry. The copper grid is mounted on the stage of a TEM which is placed in the TEM. Some waiting time is allowed until the vacuum is high enough. To get high resolution image, beam alignment procedure from top to down and purification of materials are important. The aligned beam is focused on the specimen. High resolution images of single nanowires were taken at a magnification of 9700X and beam spot size of 4 mm.

The preparation of a sample for TEM imaging involves dispersion of Si nanowires in ethanol and ultra-sonication for 15 h. One droplet of the specimen is deposited on a copper grid. The copper grid is allowed to dry in air then put onto TEM substrate holder. When the vacuum is high the beam is switched on and proper alignment procedure is carried out in order to obtain a quality image with a good contrast between particles. The beam is aligned from top to down. After alignment the beam is focused on the specimen and zoomed into the material. Fig. 4.9 shows Si nanowires and catalyst nanoparticles (Ni). The TEM results show that with laser ablation we can synthesize nanowires as small as 15 nm. The network or branched nanowires coordinated by a catalyst particle shows that nanowire growth starts on the catalysts in the plume in the furnace.

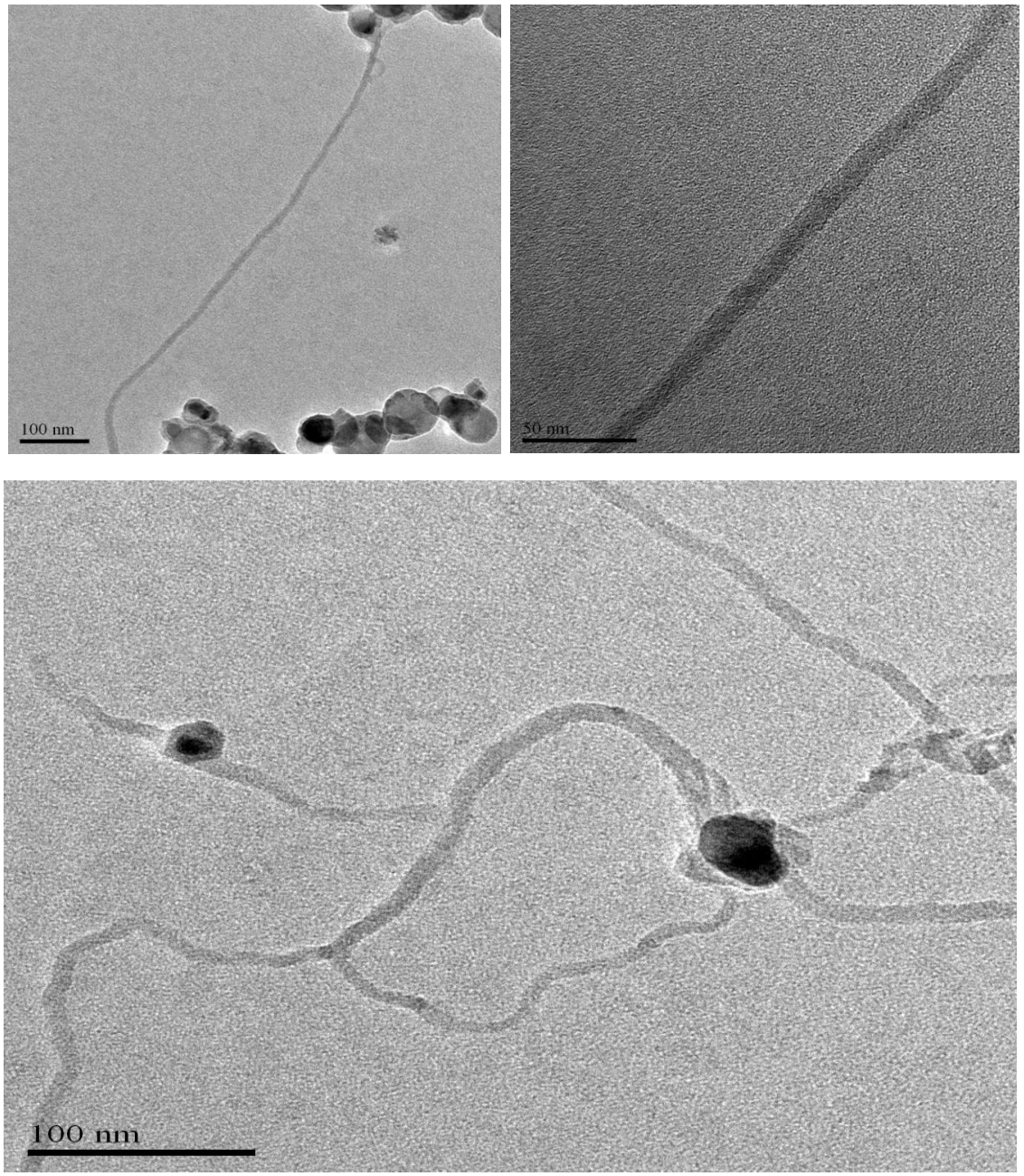

Figure 4.9: TEM images of silicon nanowires with catalyst particles.

4.2.5 Atomic force microscopy

4.2.5.1 Introduction

Atomic force microscopy (AFM) is physical microscopy technique. The AFM has a mechanical probe and this probe physically interacts with the sample. There is no focusing of light or electrons like in optical and electron microscopy. This concept makes it easy to get image with high resolution but AFM is slower than the other electron microscopies. In this project AFM was used to determine the diameter of silicon nanowires.

In this section we discuss the basic principles of an AFM, application of AFM, and how it was used to determine diameter of nanowires and their surface morphology.

4.2.5.2 Principles of AFM

AFM makes use of a laser beam that reflects from the cantilever to the detector. In AFM a probe is mounted and the cantilever tip is scanned on the sample surface by piezoelectric transducers. When the probe scans on the sample surface (in x, y and z directions) there is a force between the probe and surface and this force is sensed by force transducer and feedback control. This force varies from point to point. A varying signal is applied to the cantilever to fix the force between the surface and the tip. This signal is interpreted as an image. The AFM can be operated in tapping mode or contact mode. The cantilever alignment, probe condition, and focusing of laser beam are important for getting good image resolution. A schematic diagram of AFM is shown in Fig. 4.10 (a).

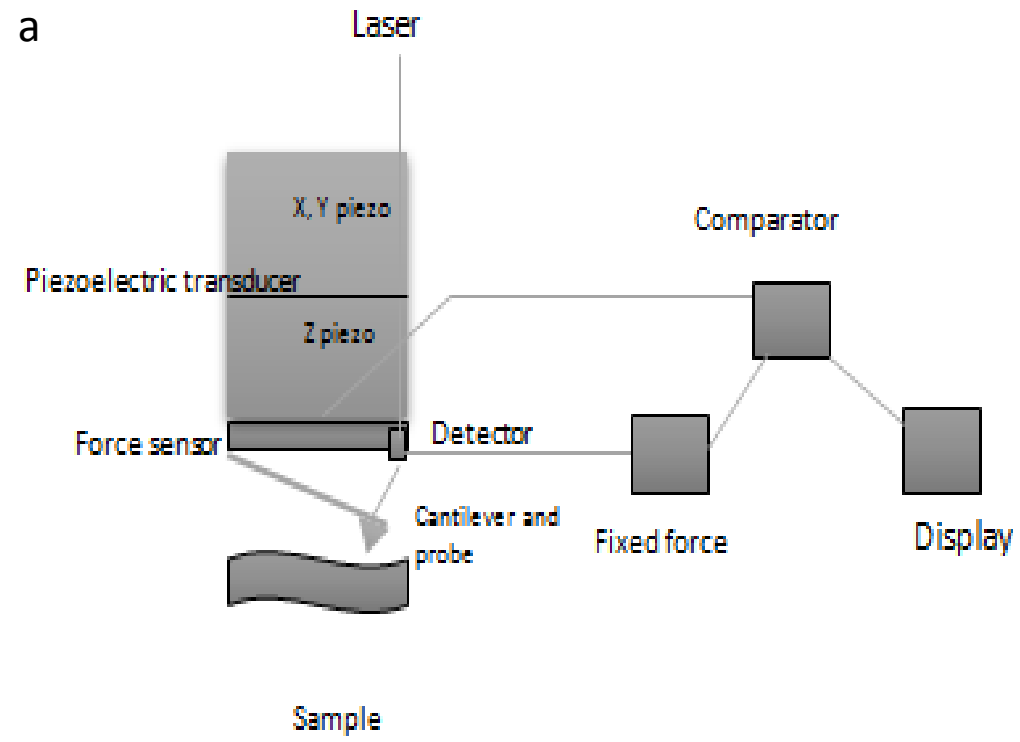

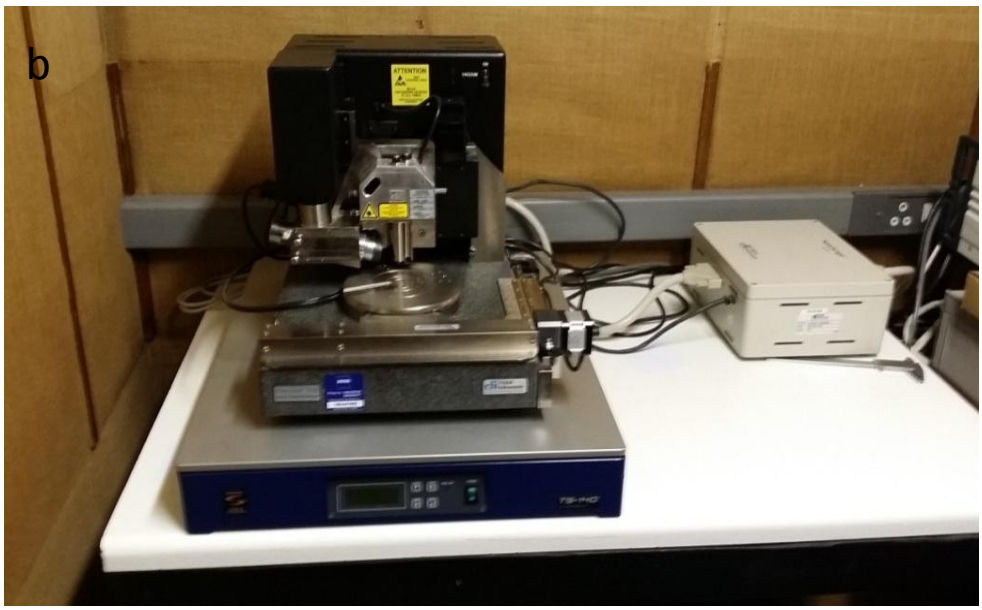

Figure 4.10: AFM images. (a) A schematic diagram of AFM. (b) The AFM instrument used in this work.

4.2.5.3 Characterization of SiNWs by AFM

We used a Veeco Dimension 3100 Atomic Force Microscope to determine the diameter of SiNWs in this study (See Fig. 4.10 (b)). Before measuring the diameter of SiNWs the AFM was calibrated. The AFM has a height resolution of 0.1 nm owing to acoustic noise. The SiNWs are sonicated for 12 h in ethanol solvent for dispersion of nanowires and then deposited on the silicon wafer then allowed to dry. The wafer is mounted on the stage of AFM anchored by a vacuum chuck. The stage is put under the cantilever and the sample is scanned. The drive frequency of the cantilever was 382 kHz. There is a CCD camera that is used for overview observation of materials which is connected to AFM. Fig. 4.11 (a) shows an AFM image of a SiNW. The diameters of the SiNWs used for making devices are given in Table 5.1.

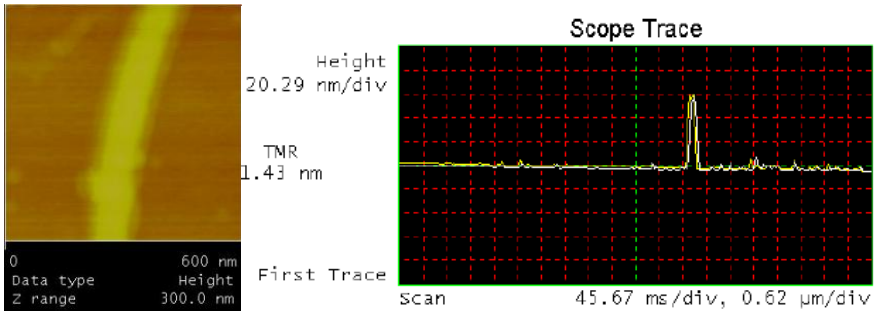

Figure 4.11: (a) AFM image of a SiNW sample B. (b) Height profile for determining diameter on nanowires.

4.3 Dielectrophoresis

In this section we discuss the principles of dielectrophoresis, a technique that was used to align silicon nanowires across two electrodes. The electric field-assisted alignment method can also be applied to align other types of NWs such as SiGeNWs and ZnONWs, normally by the dielectrophoresis (DEP) forces. The DEP forces are exerted on the dielectric NWs through induced dipoles when the NWs are subjected to a non-uniform electric field.

4.3.1 Theory of dielectrophoresis

Dielectrophoresis is based on polarization of nanowires when placed in an electric field leading to negatively charged end (n) and positively charged end (p). The axially modulated pn SiNWs, in comparison to axially homogeneous SiNWs, have not only charge neutral regions, but also charged regions. Therefore, an external non-uniform electric field can interact with the pn SiNWs both through the DEP forces on the induced dipoles and through the electrophoresis (EP) forces on the intrinsic dipoles. The combination of the DEP and EP forces determines the alignment and orientation of the axially modulated pn SiNWs. The alignment process of the axially modulated pn SiNWs is conceptually illustrated in Fig. 4.12 (a) and (b), where we have assumed that the NWs have comparable lengths to the gap distances between the two electrodes as our experiments so that the NWs bridge the gap after the alignment. When a dc electric field is applied across the two electrodes, the charge neutral regions of the pn SiNWs become polarized which are subjected to the DEP forces. The pn SiNWs also experiences the torque (T_{DEP}) generated by the DEP force when they are not parallel to the direction of the electric field. This process is demonstrated by Fig. 4.12 [60].

a

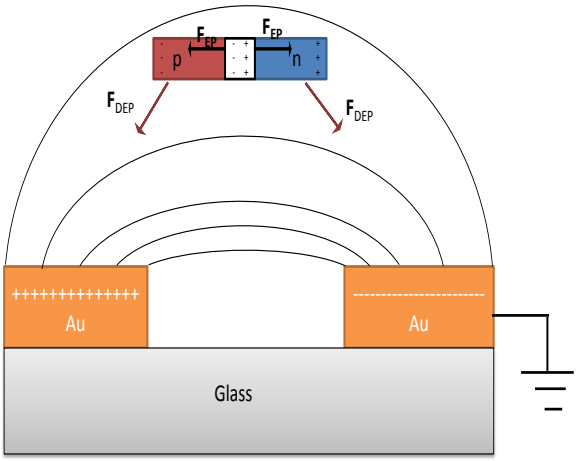

b

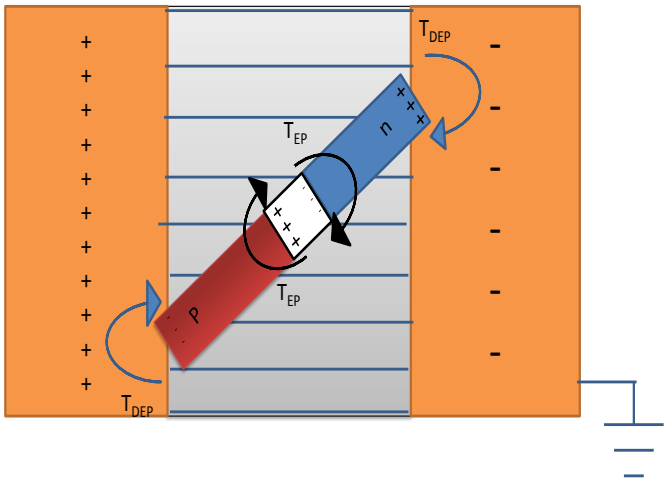

Figure 4.12: Schematics of the orientation-controlled alignment of the axially modulated pn SiNWs with an electric field. (a) The side view showing that the pn SiNW is attracted by the DEP forces toward the electrode edges where they have the largest electric field gradient, and the mass center position of the pn SiNWs cannot be changed by the two EP forces exerted on the charges in the depletion zone since they have the same magnitude but opposite direction. (b) The top view showing that the tilted pn SiNWs rotate under the combined effects of T_{DEP} and T_{EP} torques.

4.3.2 Device fabrication by dielectrophoresis

The waveguide microstructure devices used in this study for depositing and alignment of SiNWs were fabricated on glass substrate by optical lithography. The waveguide has two electrodes separated by a 1 μm gap for negative and positive bias and it has two ground electrodes which are patterned on both sides of electrodes. The microstructure glass substrate was cleaned with acetone, methanol and distilled water solvent and sonication for 10 minutes. It was then observed by optical microscopy to select good microstructures and placed under probes of DEP. The probes are connected to alternating current (ac) at 5 V_{pp} (peak-to-peak voltage) at a frequency of 1 MHz from a function generator. An optical microscope is used to visualize the alignment. A drop of the SiNWs in ethanol solvent is deposited in the gap of microstructure by a micropipette. The microstructure is blow-dried with nitrogen after the alignment. The alignment of nanowires is checked by SEM. The SiNWs are bonded to the electrodes using platinum by an OMNIGIS gas injection system and nanomanipulators are used to remove some contamination and excess nanowires that can short-circuit the electrodes to the ground lines. The purpose for using the coplanar waveguides is to allow for possible high frequency conductance measurements which have not been done yet. Fig 4.13 shows a schematic of the dielectrophoresis setup.

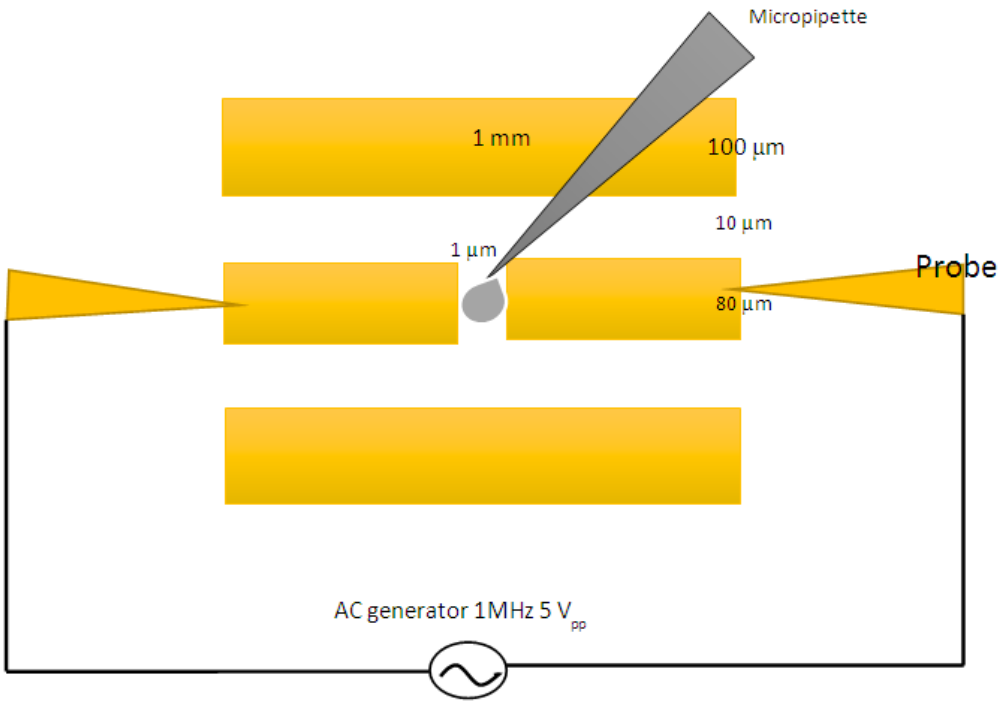

Figure 4.13: Schematic of the process of dielectrophoresis.

The aligned pn SiNWs are parallel to electric field with the p-segment contacting the higher potential side of the electrode pair (Fig. 4.14 (a)). The alignment of the SiNW is evident in the SEM image (Fig. 4.14 (b)) where all the NWs are almost parallel to each other. The density of the as-aligned pn SiNWs can be controlled through the NW concentration in the suspension. Usually there are many nanowires bridging the electrode pair. Excess nanowires are removed using a nanomanipulator as shown in Fig. 4.14 (c) so that there is only one nanowire left across the gap as shown in Fig. 4.14 (d).

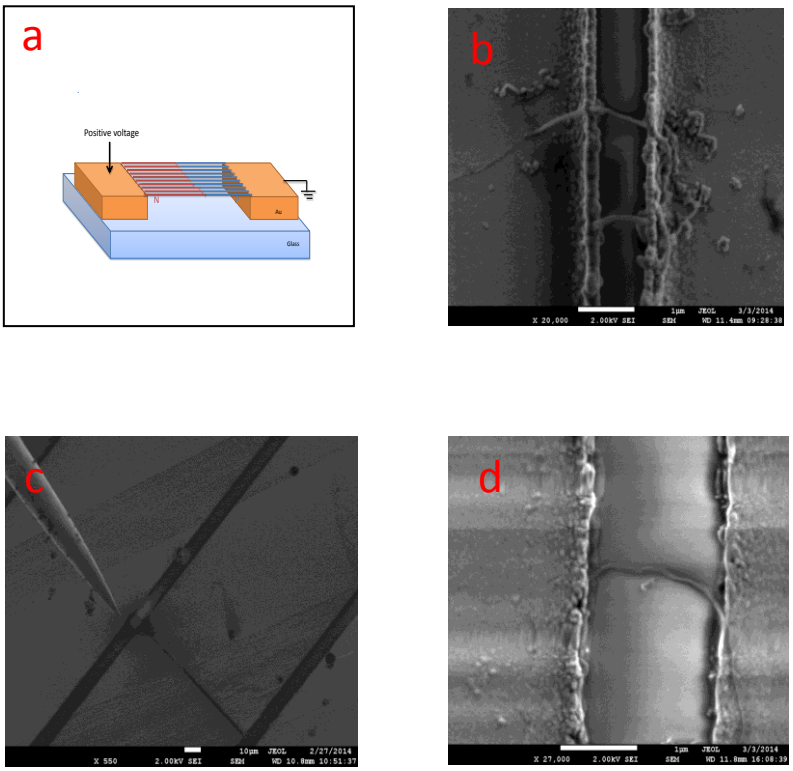

Figure 4.14: Silicon nanowires aligned across two electrodes. (a) Schematic of aligned nanowires. (b) SEM image silicon nanowires between two electrodes. (c) Removal of one nanowire using a nanomanipulator. (d) SEM Image after removal of excess nanowires showing only one nanowire remaining across the electrodes gap.

4.4 Electron-beam (e-beam) lithography

So far, we used electron beam of SEM for imaging of material but also we can use the e-beam for exposing the polymer thereby creating patterns. This is referred to as e-beam lithography. There is an addition of a beam blanker that deflect the electron beam to blank the beam between exposure events. Fig. 4.15 is a schematic of electron-beam lithography system.

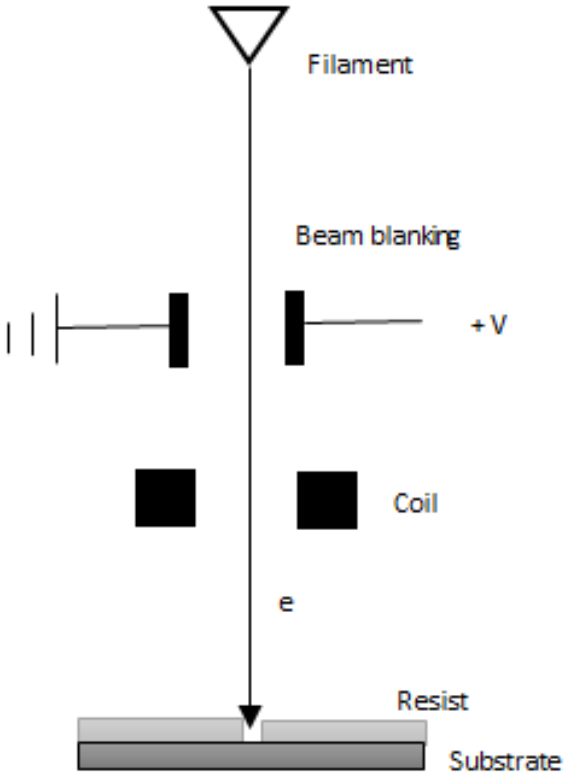

Figure 4.15: Schematic of electron beam lithography.

e-beam lithography is used in small scale fabrication. e-beam lithography is also used in the making of masks for photolithography. There are four main steps in microfabrication by PMMA lift-off based e-beam lithography. The first is the deposition of a resist, polymethylmethacrylate (PMMA), onto a planar surface by rapid spinning. The second step is exposure process which is dependent on the adjustment of acceleration voltage, focus of beam, probe current, dose factor, etc. The third step is the development process in which the exposed resist is removed by a solvent methyl isobutyl ketone. The last step is the metallization. The last step is a crucial process and its success depends on thickness of PMMA, development time that can remove all PMMA which is exposed by the e-beam in the time whilst leaving the unexposed PMMA intact. The metal is deposited using an RF sputter coater instrument (Fig. 4.16).

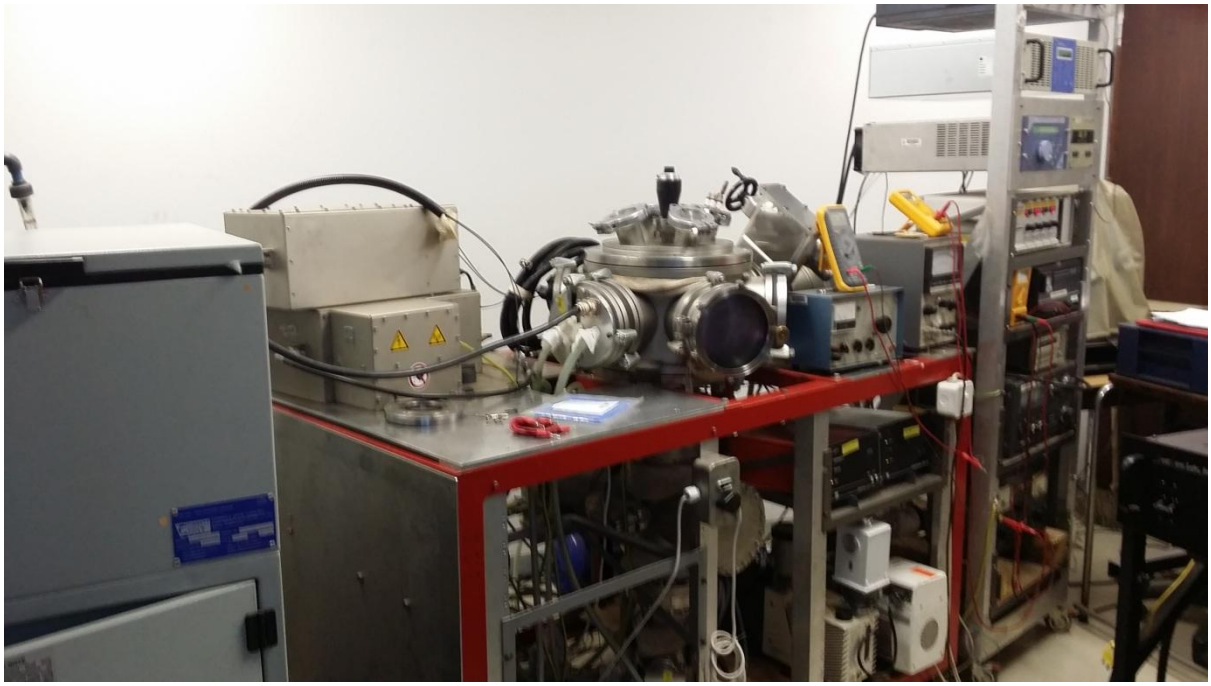

Figure 4.16: RF sputtering instrument used in the metallization of devices.

4.4.1 Fabrication of devices by e-beam lithography

In this study we fabricated devices on the SiO_2/Si substrates that have 285 nm SiO_2 and 500±25 µm Si thickness. We prepared a solution of 2% Poly (methyl methacrylate) (PMMA) of molecular weight (MW) 350 000 in Anisole solvent for making a softer PMMA layer and 2% Poly (methyl methacrylate) (PMMA) MW 950 000 in Anisole for making a harder top PMMA layer. The use of a soft and harder layer is to promote development of an undercut that makes lift-off easy. Firstly the soft PMMA is deposited on the chip and spinned at 3000 revelation per minute (RPM) for 1 min and baked at 160 ^{o}C for 4 min. The thickness of PMMA layer is about 50 nm and this is repeated 4 times to obtain a thickness of 200 nm. The harder PMMA layer is deposited in the same way and repeated 2 times to get a thickness of 100 nm. We used a 6800 Spin Coater instrument. The chip is then mounted on the stage of SEM and placed in the SEM chamber and then the SEM is switched ON. The acceleration voltage is set to 30 kV and the probe current is set to 1 nA. The following are the steps of the exposure:

1. Designing of pattern and layers:
    a. Set Working area to 1x1 mm.
    b. Define the different layer.
2. Angle correction
3. Origin correction
4. Beam optimization.
5. Beam blanker ON.
6. Patterning:
    a) Open positionlist (new positionlist).
    b) Drag and drop design.
    c) Select the layer.
    d) Change define pattern position (in property list)
        i. Correct position.
        ii. Set exposure parameter and calculate exposure time.
        iii. Click ok.

7. Create Matrix (Filter matrix copy).
8. Set magnification.
9. Click scan.

After exposure process, the pattern is developed by putting the chip into methyl isobutyl ketone for 30 seconds then 5 seconds in IPA followed by blow drying by nitrogen gas. The next step is metallization by depositing 4 nm titanium and 40 nm gold using a sputter coater instrument and then doing a lift-off process by dipping the chip in acetone about 12 hours and then ultrasonicating for 5 minutes. The Fig. 4.17 illustrates the lithography procedure.

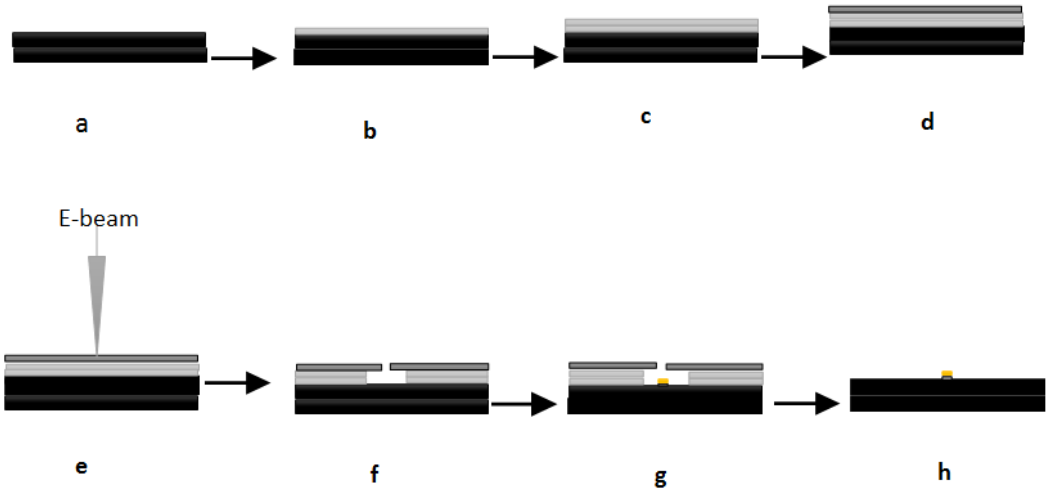

Figure 4.17: Electron beam lithography. Image a, b, c, d, e, f, g and h show SiO2/Si chip, the chip with a soft PMMA layer deposited and baking 4 minutes, the deposition of second PMMA layer and baking 4 minutes, deposition of hard PMMA layer and baking 4 minutes, exposure by e-beam, developing, metalize and lift-off by acetone respectively.

There is an additional procedure to align electrodes onto the nanowires, the bonding pads and larger electrodes. This alignment process involves use of a 3-point correction and 4-point alignment using manual marks that are pre-patterned on the chip. Fig. 4.18 show devices developed by e-beam lithography.

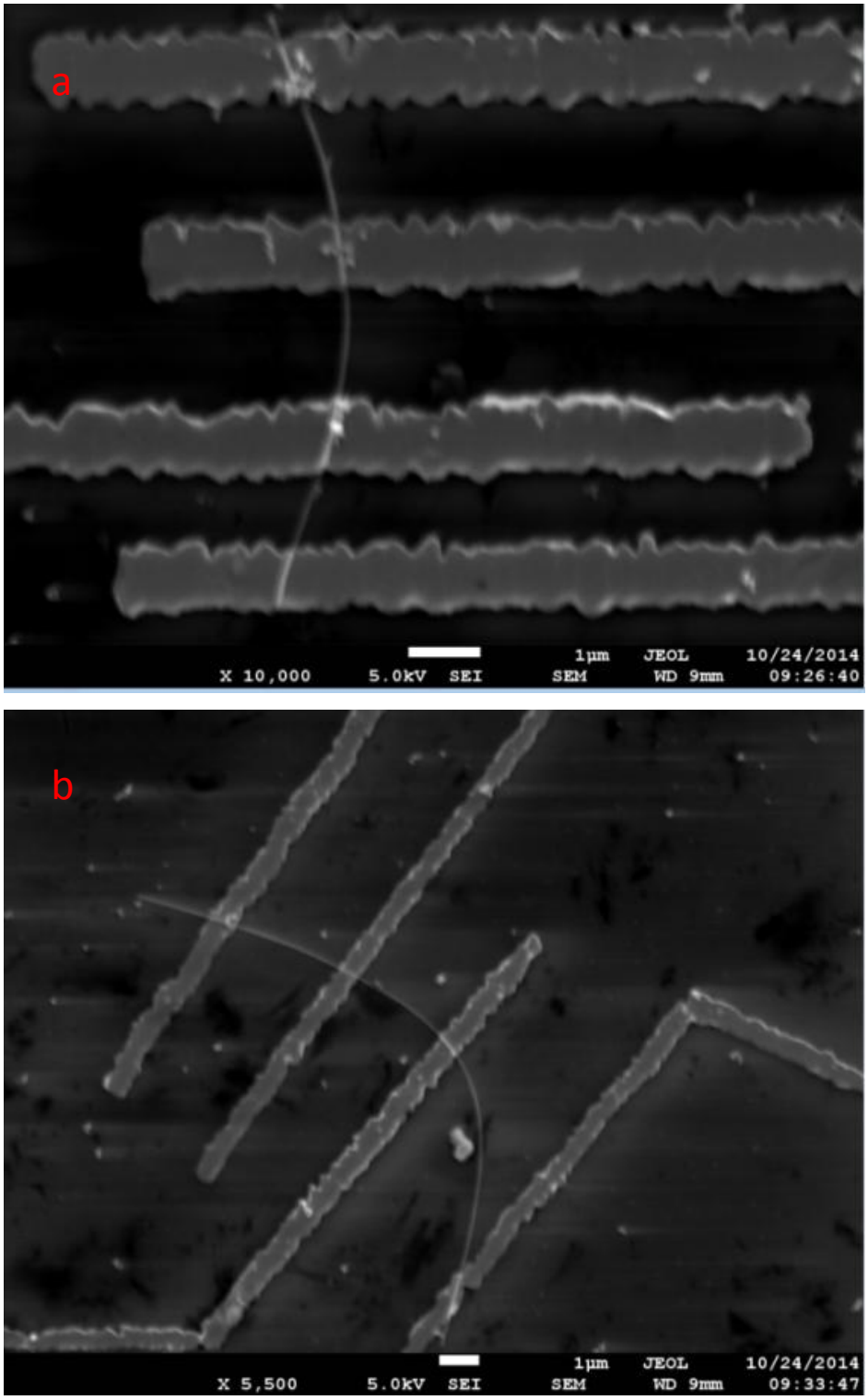

Figure 4.18: SEM image of a silicon nanowire 4-terminal device (a) sample B and (b) sample C. The 4 terminals are used for 4-wire sensing (Kelvin) measurement technique in which current is passed through the two outer electrodes and a voltage drop is measured across the two inner electrodes. The devices were made using e-beam lithography.

4.5 Current-voltage measurement

In this study, we used an Agilent B1500A Semiconductor Device Analyzer for current-voltage measurements. The device that is fabricated by DEP is placed on the Janis probe station. This experiment is done under high vacuum which is 10^{-6} Pa that is achieved with a BOC Edwards Turbo pump. Liquid nitrogen is added, the nitrogen pass through into the chamber with running the pump. The liquid nitrogen transfer causes the temperature in the chamber to go down to 77 K. There are two metal tips which have ability to move in three directions (x, y and z). When the temperature is at 77 K, the tips are landed on the device gently under a stereo microscope and the measurement is started in the dark to avoid contributions of photon assisted currents. The Semiconductor Analyzer has a desktop computer and uses EasyEXPERT program for measurements. Fig. 4.19 shows a device under the tips on the probe station in the chamber.

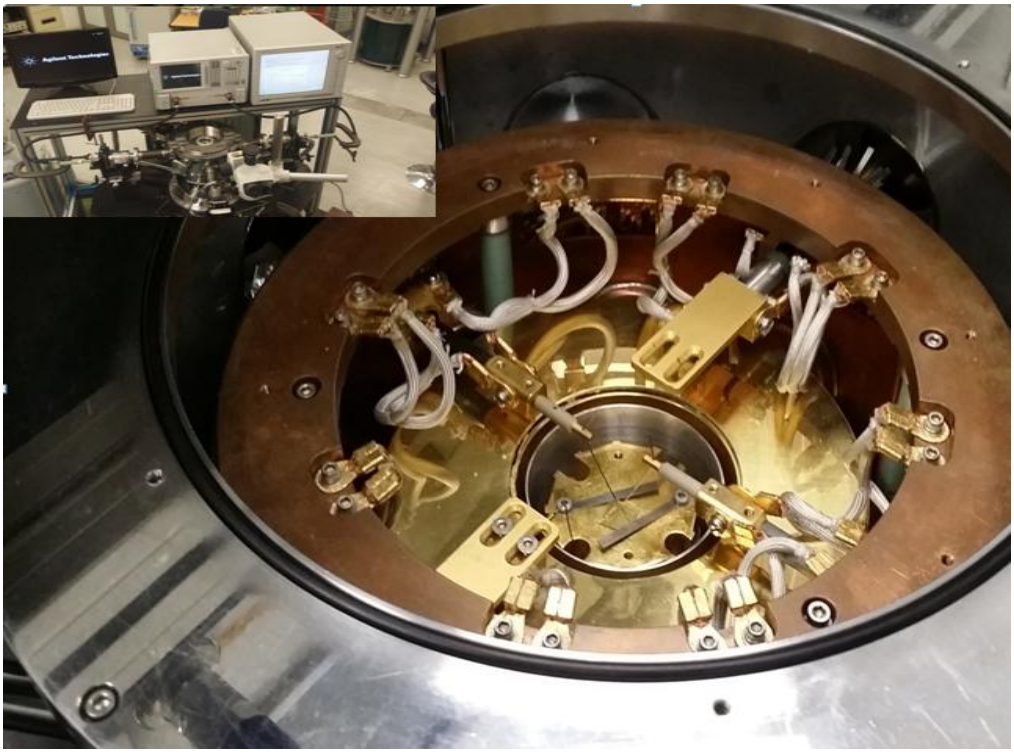

Figure 4.19: Current-Voltage measurement setup. The device is placed on the probe station. Inset shows a semiconductor analyzer used for I-V measurements.

4.6 Temperature Dependent and Magnetic Field Dependent Measurements

We fabricated four-terminal devices by e-beam lithography for low temperature electronic characterization in a Cryogenics system. In this study, we measure resistance in the temperature range 2 K to 300 K and magnetoresistance in the magnetic field range 0 to 12 T at different temperatures. The device is mounted onto the variable temperature insert (VTI) of a Cryogenics measurement system and the VTI is interfaced with the measurements rack via a break-out box. The measurements rack contains a desktop computer, a Keithley 2400 source-meter and a Keithley 2182A nanovoltmeter, a magnet power supply and a temperature controller. A LabVIEW program is used in the control of the hardware and in the data acquisition. The Cryogenics measurement system is shown Fig. 4.20. In the four-probe measurement a current of 1 to 10 μA is passed through the nanowire through terminals 1 and 4 and a voltage drop is read across the terminals 2 and 3. This takes out the contribution of resistance from the measurement leads as would be the case in a two-probe measurement.

Figure 4.20: Cryogenics measurement system for low temperature and high magnetic field measurements.

5 RESULTS AND DISCUSSION

5.1 Temperature dependence of resistance of silicon nanowires

In table I the different samples on which electrical transport measurements were done are listed. Generally the room temperature resistance of the samples ranged from 1.7 kΩ to 10 kΩ whereas the low temperature resistance ranged from 3.4 kΩ to 75 kΩ. The temperature dependence of sample A is shown in Fig. 5.1 (a) and that of sample B in Fig. 5.1 (b) and that of sample C in Fig. 5.1 (c). In general the resistance is gradually decreasing with increase in temperature. Fitting exponential curves we find that the resistance of the devices A and C is governed by the Arrhenius type thermally activated transport in which $R \propto \exp\left(E_g / 2k_B T\right)$. The bandgaps of these devices are estimated to be 11 meV and 41 meV respectively. The sample B has a peculiar temperature dependence with three distinct regions in the RT curve. In region 1 the resistance drops sharply with increasing temperature whereas in region 2 the resistance stays almost flat in the temperature range 25 K to 150 K (Fig. 5.1 (b)). The flattening of the resistance as the temperature is decreased can be attributed to a lowering phonon scattering that competes with Arrhenius transport behaviour. Similar temperature dependence has been observed in polycrystalline InSb doped with Bi and Pb [52]. Region III exhibits a down turn in the resistance with increasing temperature as expected in the Arrhenius thermally activated transport. Our RT data did not fit variable range hopping models observed in sub10 nm p-type doped nanowire [62]. This may be attributed to reduced disorder due to lack of doping.

Sample	$R_{300\,K}$ (kΩ)	E_g (meV)	Length (μm)	Diameter (nm)
A	10	11	1	-
B	1.7	-	1.5	55
C	1.8	41	3	45

Table 5.1: Room temperature transport characteristics of samples developed in this work. The diameters of sample B and C were determined by AFM.

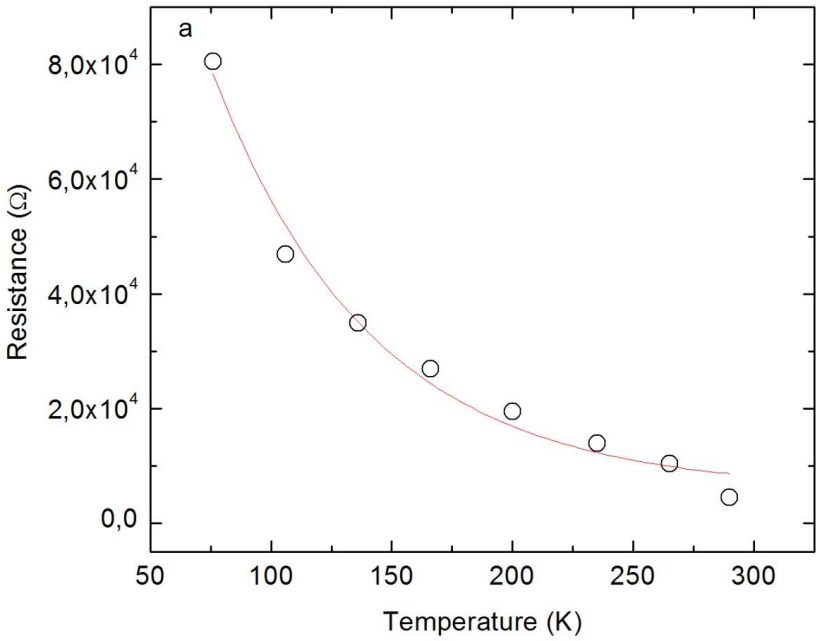

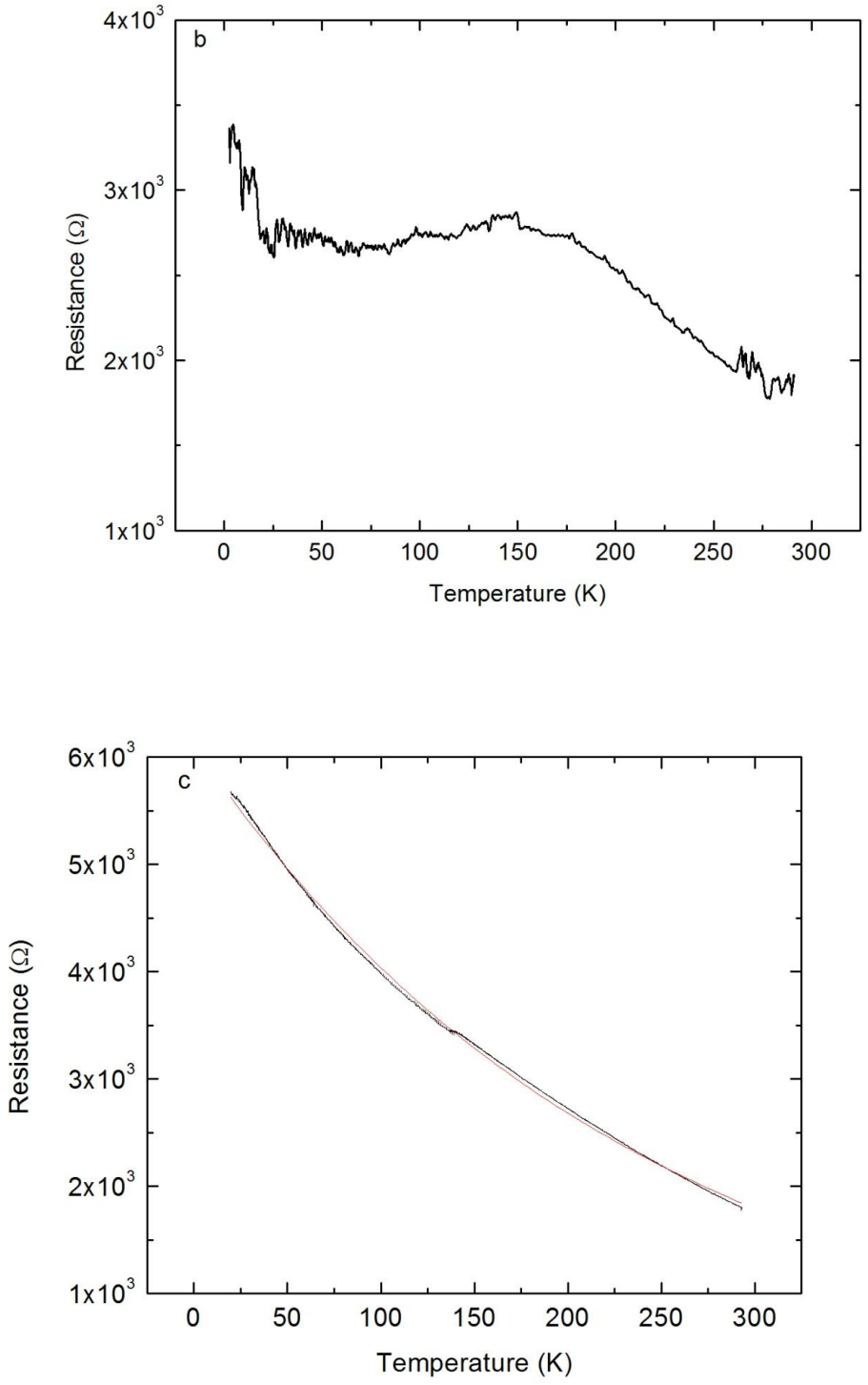

Figure 5.1: Temperature dependence. (a) R-T characteristics for SiNWs (Sample A) aligned across a 1µm gap by DEP and contacted by GIS metallization technique. The red curve is an exponential fit to the data. (b) Temperature dependence of resistance of sample B fabricated by lift-off based e-beam lithography. (c) Temperature dependence of resistance of sample C fabricated by lift-off based e-beam lithography. The red curve is an exponential fit to the data.

5.2 Current voltage characteristics

The current-voltage (I-V) characteristics of samples were also taken. Fig. 5.2 (a) shows the I-V characteristics of a device (sample A) fabricated by DEP and GIS metallization technique. The I-V curves are non-linear even at room temperature. This nonlinear behavior is expected for semiconducting devices. The I-V curves of sample A become moderately non-linear as temperature is decreased. The I-V curves of sample B are weakly non-linear at low temperature (Fig. 5.2 (b)). This is in good agreement with the low resistance observed in this sample. The I-V characteristics of sample C are strongly non-linear with threshold voltages > 10 V on the positive bias side and < 10 V on the negative bias side. Conductance steps can also be observed in the I-V curves at 2.7 K and 5 K (Fig. 5.2 (c)). This a signature of quantum transport of silicon nanowires. The current steps may also be related to an onset of negative differential resistance in the nanowire. More pronounced peaks are observed in the plot of differential conductance (d*I*/d*V*) versus bias voltage (Fig. 5.2 (d)). This is a signature of resonant tunnelling conduction.

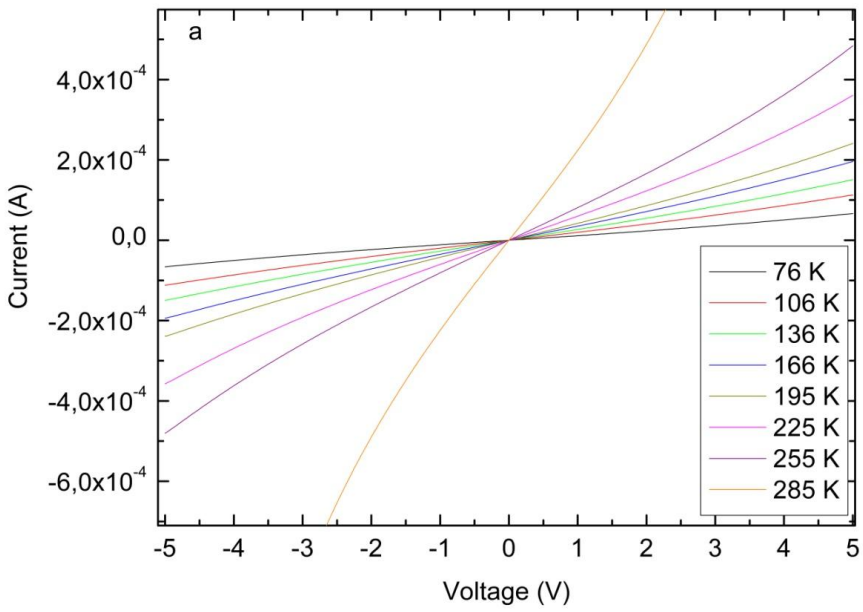

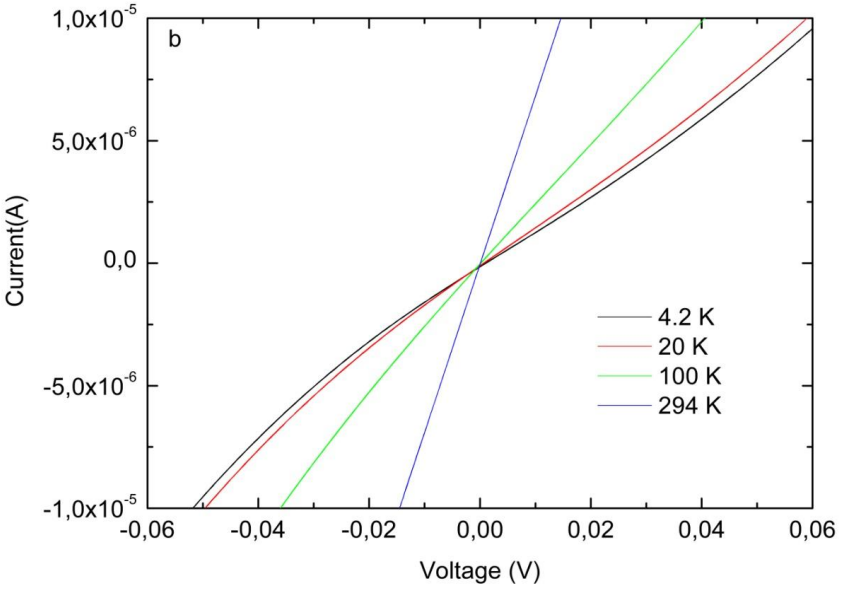
b
1,0x10-5
5,0x10-6
0,0
-5,0x10-6
-1,0x10-5
Current(A)
-0,06
-0,04
-0,02
0,00
0,02
0,04
0,06
Voltage (V)
4.2 K
20 K
100 K
294 K

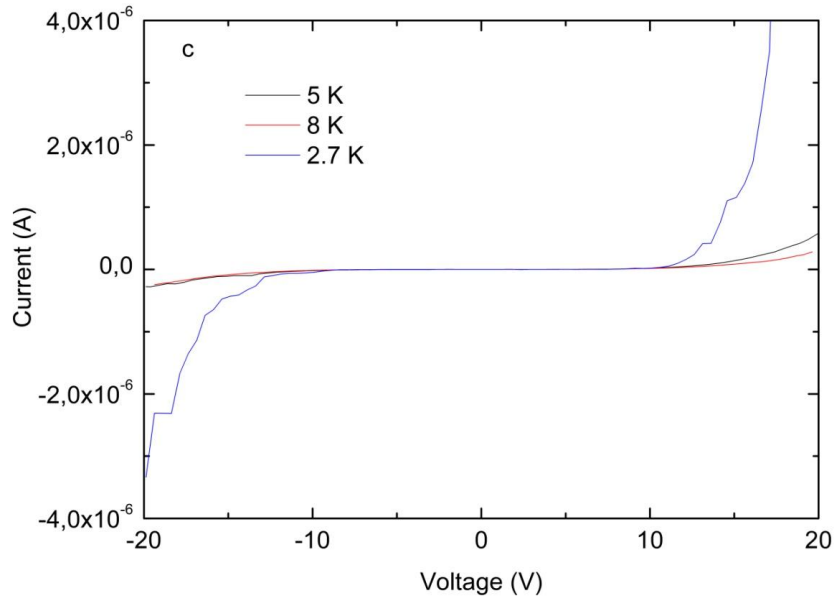
c
4,0x10-6
2,0x10-6
0,0
-2,0x10-6
-4,0x10-6
Current (A)
-20
-10
0
10
20
Voltage (V)
5 K
8 K
2.7 K

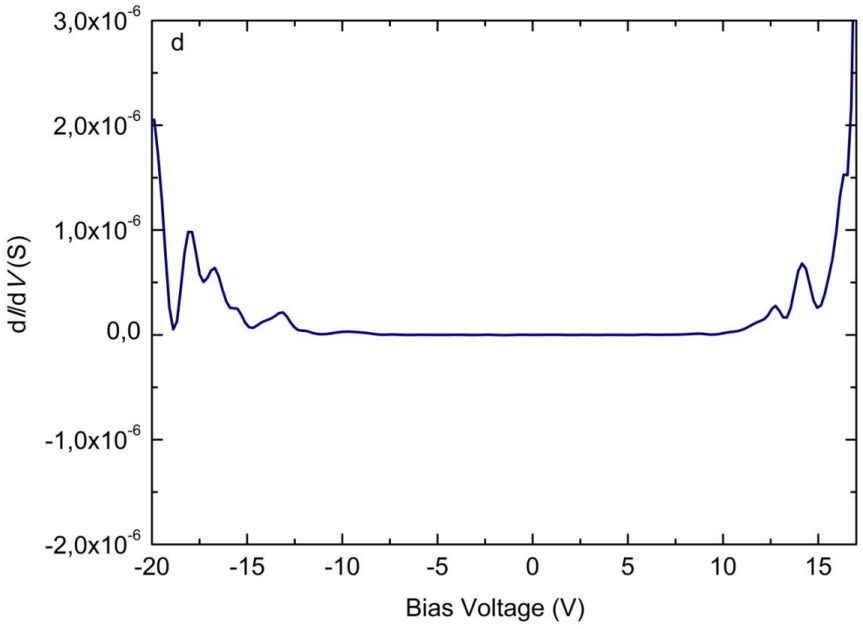

Figure 5.2: I-V characteristics of (a) sample A, (b) sample B and (c) sample C at various temperatures. (d) Differential conductance as a function of bias voltage for sample C that exhibited step like features at 2.7 K.

5.3 Magnetoresistance of silicon nanowires.

We examine the magnetoresistance due to a magnetic field applied perpendicular to the SiNW. Magnetoresistance is defined as $MR = \frac{R(B) - R(0)}{R(0)}$

where $R(B)$ is resistance which change with field and $R(0)$ is the resistance at zero field. There are two notable features of the magnetoresistance shown in Fig. 5.3 (a) - (d). Firstly, a non-saturating linear positive MR is observed as shown in Fig. 5.3 (a) for a 3 μm long, 45 nm wide silicon nanowire (sample C). Here the resistance of the sample increases linearly as the magnetic field is swept from 0 to about 10 T. The slopes of MR lines are 0.005, 0.013 and 0.021 for 100 K, 10 K and 2.5 K, respectively. The increase in slope with the decrease of temperature indicates that charge carriers are more easily localised into cyclotron orbits at lower temperature. The positive MR is due to the creation of increasingly smaller cyclotron orbits as the magnetic field is increased, this has the effect of increasing the resistivity of the sample. As can be seen in Fig. 5.3 (a), the linear background is greatly reduced as the temperature is increased.

In Fig. 5.3 (b) for a 1.5 μm long, 55 nm wide nanowire (sample B) a saturating positive MR is observed. The saturation of the MR with increase in field can be attributed to the limiting of the extent to which the cyclotron radius can be reduced. This is related to flux quantization that is to say there is a limit to the smallest flux that can enclosed by an orbiting electron.

The second noteworthy feature is that of oscillations in all the magnetoresistance plots. This oscillatory behaviour persists at temperatures 10 K and 100 K. The oscillations are irregular (with beating) more pronounced in sample C at 100 K with approximate period of ~ 2 T for major peaks and ~ 60 mT for the finer oscillations. These periods correspond to cyclotron radii of ~18 nm and ~104 nm. It is not hard to imagine the prevalence of circular 18 nm orbits within a 45 nm wide nanowire. However a circular 104 nm orbit cannot fit into a 45 nm nanowire unless it is of elliptical or other irregular shape. Therefore we may not associate the 60 mT oscillations to magnetic field induced circular cyclotron orbits in the bulk of the wire. The phase coherence length (L_φ) associated with the periodicity, estimated using formula $\Delta B = \phi_0/L_\varphi^2$ where $\phi_0 = \frac{\hbar}{2e} = 2.068 \times 10^{-15}$ Wb is the flux quantum, is found to be 32 nm and 185 nm (for ΔB~2 T and 0.06 T respectively) at 100 K [65]. Dividing the phase coherence lengths by the Fermi velocity (1×10^7 m/s) we obtain quantum lifetimes in the range 3 to 19 fs. This is significantly small compared to scattering lifetime of 1 ps of bulk silicon [66] and indicates either the presence of large number of impurities or a large extent of surface roughness scattering in silicon nanowires.

From the magnetoresistance oscillations we can extract the effective mass of carriers in the silicon nanowires. To do this, we first plot the resistance as a function of $1/B$ as shown in Fig. 5.3 (c). The separation $\Delta(1/B)$ between SdH-like peaks is plotted as a function of $1/B$ minima in Fig 5.4 (a) inset. The carrier concentration n_s is calculated from the formula $\Delta(1/B) = 2e/n_s h^2$ and plotted against B in Fig. 5.4 (a). The carrier concentration is found to scale linearly with B for all temperature points. The increase of n_s with B can be attributed to the increase of degeneracy of Landau levels, $n_L = 2\frac{e}{hc}AB$ where A is the area of the nanowire perpendicular to the magnetic field. Similar scaling of carrier concentration with B has been observed in other materials

such as graphene [67]. The carrier density values in the range 2×10^{11} cm^{-2} to 9×10^{12} cm^{-2} correspond to effective mass $m^* = (\frac{\hbar}{v_F})\sqrt{\pi n_s}$ that varies from 0.001 m_e to 0.006 m_e (where m_e is the free electron mass) in the temperature range 2.5 K to 100 K and field range 1.5 T to 10 T. These n_s values are comparable to carrier concentration of the order 10^{12} cm^{-2} measured in multi-walled carbon nanotubes under transverse magnetic field [68]. The concentration of static scattering centers is estimated to be in the range 27 to 1200 cm^{-2} using the slopes of the MR data at 2.5 K in Fig. 5.3 (a) and the generic description of linear quantum magnetoresistance given in equation 2.14 [51,52].

To extract the quantum lifetime we make use of the general form of magnetoresistance of a low dimensional system in the SdH oscillation regime which is given by [65]:

$$R_{XX} = R_0\left[1 + \lambda\sum_{S=1}^{\infty} D(sX)exp\left(-\frac{s\pi}{w_c\tau}\right)\times\cos\left(s\frac{\hbar S_F}{eB} - s\pi + s\phi_0\right)\right] \qquad (5.1)$$

From which to the first order we can write the amplitude of oscillations as: $A_{ex} = \lambda D(X)exp\left(-\frac{\pi}{w_c\tau}\right)$, where $w_c = eB/m^*$. The carrier lifetime can be calculated by plotting the amplitude of the oscillation versus the $1/B$ at extrema of oscillations as shown in Fig. 5.4 (b) for 100 K. Using the slope of this graph and the value of effective mass obtained earlier we estimate the carrier life time as 13 fs. This value is of the same order of magnitude as quantum lifetimes measured in other low dimensional systems such as single layer graphene [69].

In the case of an applied perpendicular magnetic field it would be expected to observe harmonic SdH oscillations at low temperature as observed in graphene [69] and other 2DEG systems [70]. Usually in these oscillations the amplitude increases with increasing magnetic field due to smaller cyclotron orbits forming at higher fields as the Landau level crosses the Fermi level resulting in more of the edge state electrons being localized by the magnetic field [43]. However, in our sample, the oscillation amplitude is independent

of magnetic field and remains constant even at high fields. This anomalous behaviour can be explained as follows; Application of magnetic field perpendicular to the nanowire axis leads to formation of three different electron orbital motion: pure orbits, skipping orbits and also traversing orbits (Fig. 5.5). In a 2D system and also in wide nanowires the pure orbits will become smaller and smaller as the magnetic field is increased thus leading to a conventional SdH oscillations with amplitude that increase with increasing field. However in narrow quantum wires the pure orbits in the core or bulk of the quantum wire are pinned by disorder or impurities. In other words, as the magnetic field is increased to a point that corresponds to a Landau level matching the Fermi level, edge states can be converted to cyclotron orbits. This conversion is however prevented due to backscattering resulting from impurities in the bulk of the nanowire. Due to this, an increase in the magnetic field does not necessarily lead to increasingly smaller cyclotron orbits to form, due to the electrons forming these orbits being scattered, and hence leads to oscillations of constant amplitude.

The lack of smearing or damping of the MR oscillation in Fig.5.3 (a) at temperature as high as 100 K prompts us to check whether the magnetoresistance oscillation may be just universal conductance fluctuations (UCF) which have been observed in a wide range of mesoscopic scale materials. UCFs are known to scale with length as $\Delta G = \frac{\Delta R}{\langle R \rangle} \approx \frac{e^2}{h}\left(\frac{l_\varphi}{L}\right)^{3/2}$ [71]. Using this relationship we obtain phase coherence lengths of 1.5 μm, 1 μm and 0.012 μm for 100 K, 10 K and 2.5 K, respectively. The decay of coherence with decreasing temperature is contrary to the expectation of improved coherence with lowering temperature in systems where phonons are the main phase breaking mechanism. Therefore these oscillations cannot be explained by UCF. It should be noted that high temperature magnetoresistance oscillations have before been observed in InGaAs quantum wells and it is not surprising to see the manifestation here [61]. These oscillations were attributed to transverse acoustic-phonon assisted transitions between magnetically induced states above the quantum well and a shallow impurity well.

We next consider the possibility of an AB effect origin of the oscillations for magnetic field oriented perpendicular to SiNWs. AB oscillations have been previously reported in multiwalled carbon nanotubes under magnetic field applied perpendicular to the nanotube but have not been reported in individual SiNWs [72]. Assuming that the large period oscillations (~2 T) observed in sample C correspond to AB oscillations the area of the AB loops/rings for this period is 6.6×10^{-16} m^2 (i.e. a ring diameter of 52 nm). Such a ring diameter is comparable to the diameter of the nanowire determined by AFM (45 nm). A zoom into the conductance fluctuation of sample C (D~45 nm, L~3 μm) (Fig. 2(d)) reveals fine Aharanov-Bohm-like oscillation of periods 20 mT. The 20 mT period correspond to an AB ring of area ($A=2\pi\hbar/e\Delta B$) of 2.1×10^{-13} m^2 corresponding to a ring radius of 260 nm. AB loops of this area will only fit into a silicon nanowire if they were of elliptical shape with a minor axis of 45 nm and a major axis of at least 2.9 μm. A zoom into the conductance fluctuation of sample B (D~55 nm, L~1.5 μm) (Fig. 5.3(d)) reveal fine AB-like oscillation of periods 60 mT. The AB oscillation may arise from interaction between the magnetically induced pure orbits in the core of the nanowire and propagating edge states at the surface of the nanowires [66]. The 60 mT period correspond to an AB ring of area of 6.9×10^{-14} m^2 corresponding to a ring radius of 140 nm. AB loops of this area will only fit into a silicon nanowire if they were of elliptical shape with a minor axis of 55 nm and a major axis of at least 1.6 μm. The lengths of the major axes for AB ellipses (2.9 μm and 1.6 μm) are comparable to the lengths of the silicon nanowire device (3 μm and 1.5 μm). Thus, we may then associate the oscillation periods 20 mT and 60 mT to the AB phase of edge states which propagate ballistically through the wire and only scatter near the contacts. Using the relation $\Delta(1/B) = 2\pi e/\hbar A_{FS}$ we find that the range of $\Delta(1/B)$ 0.011 to 0.3 T^{-1} corresponds to the cross sectional area of a Fermi surface pocket (A_{FS}) in the range 3.2×10^{16} to 8.7×10^{17} m^{-2} in k-space. However the exact morphology of the Fermi surface pockets is not understood.

The irregularity in the MR oscillations indicate that there may be many possible contributions to the oscillatory behaviour. There may be

magnetointersubband oscillations due to impurity assisted scattering as well as phonon induced resistance oscillations due to phonon assisted scattering in addition to SdH oscillations and universal conductance oscillations. A more systematic study of the MR behaviour is required to establish the dominant mechanism. This can include the study of MR oscillations as a function of bias current and gate voltage. Higher bias currents are expected to increase electron temperature which can lead to phase decoherence. By varying the current one can change the phase of the electron wavefunctions in a controllable way that can be manifested as changes in the oscillation period.

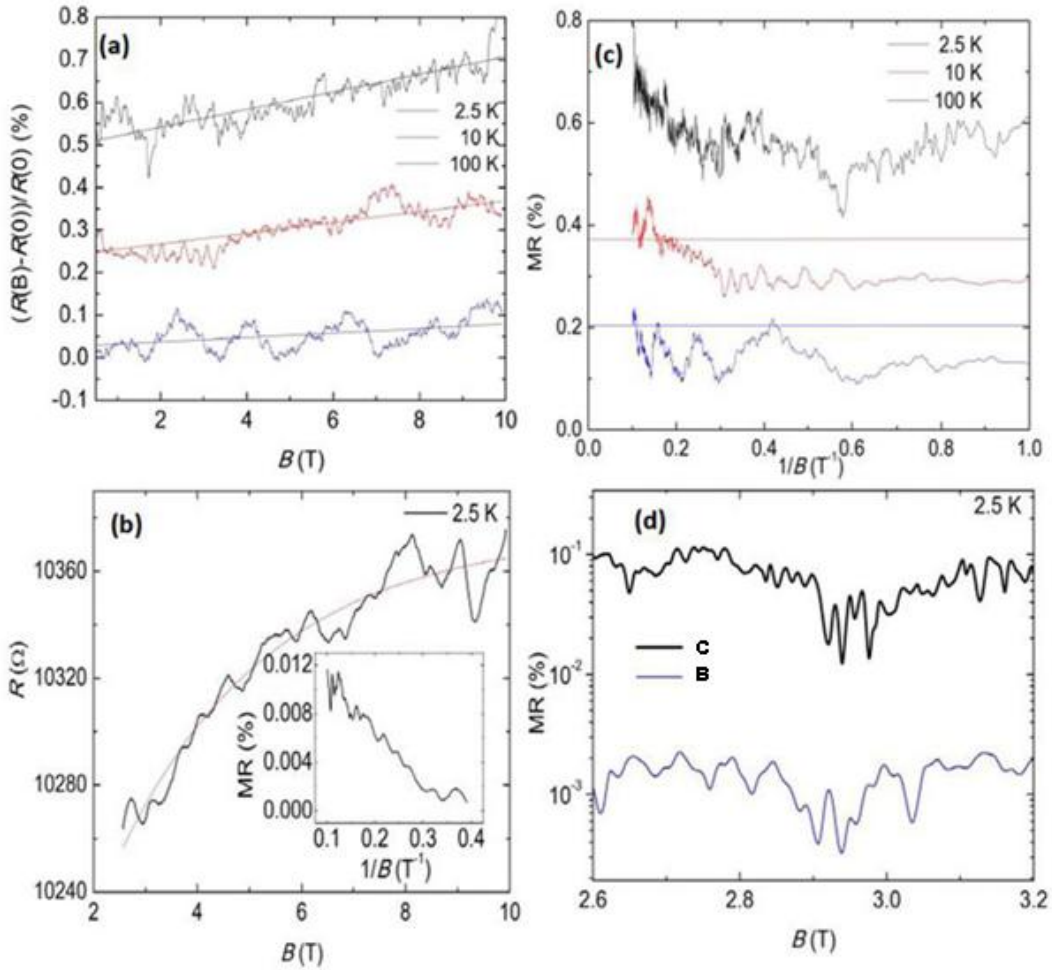

Figure 5.3: (a) Transverse magnetoresistance of sample C (diameter 45 nm and length 3 µm) at various temperatures 2.5 K (black line), 10 K (red line) and 100 K (blue line). The MR curves have been offset by 0.5, 0.3 and 0.1 % for clarity. Oscillations are observed in all the magnetoresistance curves. (b) A saturating positive magnetoresistance is observed in sample B with diameter 55 nm and length 1.5 µm. (c) Variation of resistance with 1/B for sample C at 2.5 K, 10 K and 100 K. Note: The curves in (c) have been offset upwards for clarity. The amplitudes don't vary much with field and the oscillations are more AB like at 2.5 K. The oscillation amplitude are more pronounced in the intermediate and higher field regions at 10 K. The oscillations appear SdH-like with strong amplitude at higher field. (d) AB-like oscillations in the field range 2.5 to 4 T for sample C (black curve) and sample B (blue curve)

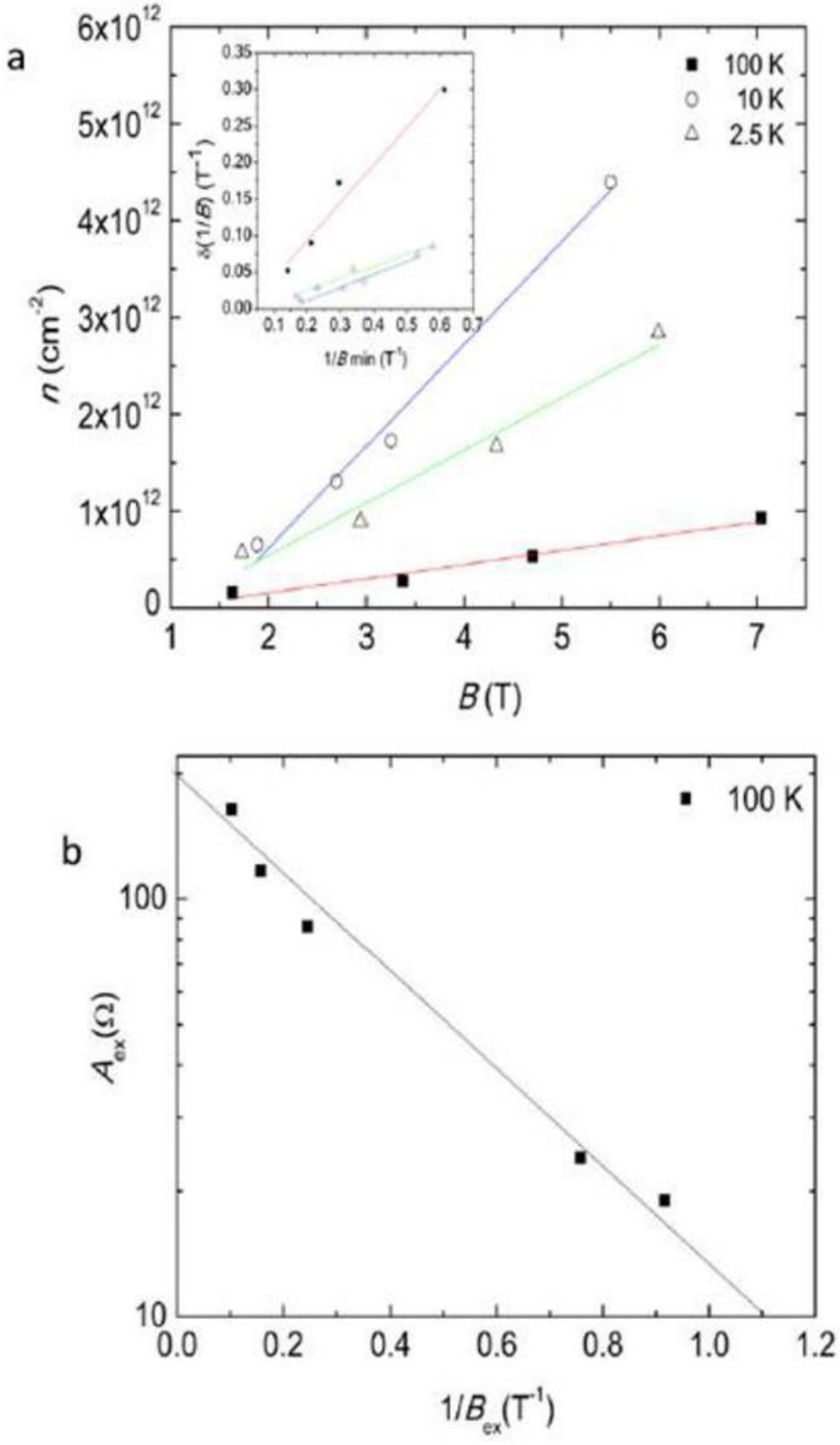

Figure 5.4: (a) The variation carrier density with magnetic field at various temperatures in sample C. Inset: Variation of peak spacing with 1/B minimum used to calculate the carrier density. (b) The variation of amplitude of extrema points of the resistance oscillations versus 1/B used to extract the quantum lifetime.

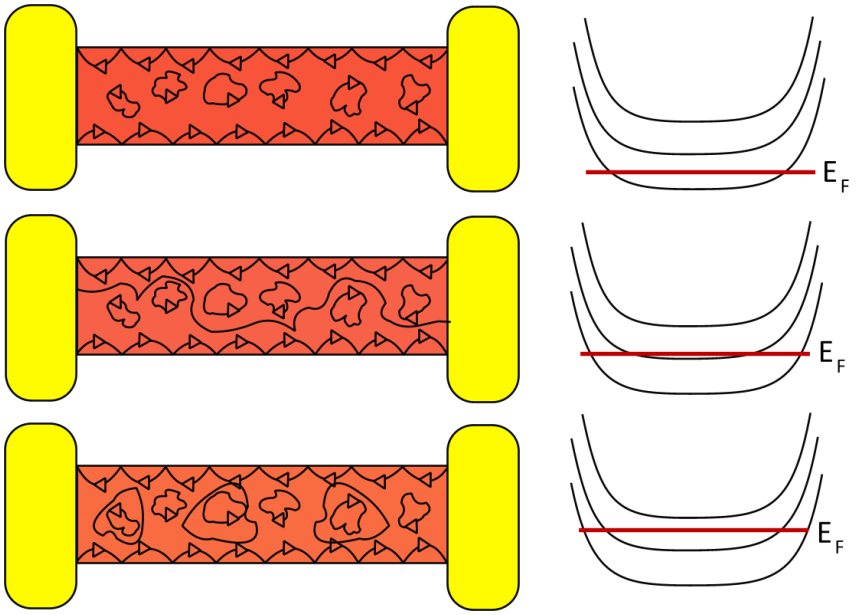

Figure 5.5: Schematic diagram showing the edge states, impurity pinned orbits as well as the corresponding landau level interpretation [43].

6 CONCLUSIONS AND RECOMMENDATIONS

6.1 Synthesis of nanowires by laser ablation

Our experimental work demonstrates the method of synthesizing silicon nanowires by laser ablation using nickel as the catalysts. Long and clean nanowires (up to 5 μm) can be obtained. However, there were many nanowires which were unclean or contaminated with catalyst particles and these were not used for device fabrication. Using dielectrophoresis and e-beam lithography two-terminal and four-terminal devices can be made.

6.2 Electronic transport behaviour

The electronic transport behaviour at zero magnetic field was found to be predominantly Arrhenius type thermally activated transport with bandgaps in the range 11 meV to 41 meV. The magneto-transport for these devices was also probed; it was found that in these nanowires a positive linear magnetoresistance is observed alongside anomalous magnetoresistance oscillations with amplitude being independent of both temperature and field. The temperature and magnetic field independence can be attributed to quantum interference effects between skipping orbits, which penetrate into the core as an occupied Landau level is moved through the Fermi level, and pure cyclotron orbits pinned throughout the nanowire by impurity scatterers. The irregularity of the oscillations suggests a presence of many other contributions to the oscillatory behaviour such as magneto intersubband oscillations and phonon induced resistance oscillations.

6.3 Recommendations

Save for a few nanowires on which device were many of the nanowires synthesized in this work were unclean with some coatings on their surfaces. In the future procedures for purification or cleaning of the nanowires need to be developed. Doping of the nanowires and development of small diameter silicon nanowires will be pursued in our future work on nanowires.

The zero magnetic field measurements included measurements of current voltage characteristics and temperature dependence of resistance. Future studies should include measurements of field effect transistor parameters utilizing the backgate provided by the silicon layer underlying the devices.

Our magnetoresistance measurements were only done on the positive magnetic field side and the field were applied perpendicular to the nanowires. Future studies should include measurements of magnetoresistance on both positive and negative magnetic field sides and the angular dependence of magnetoresistance should be studies. In the light of many possible contributions to the magnetoresistance oscillations a more systematic study of the MR behaviour is required. This should include the study of MR as a function of bias current and gate voltage.

7 REFERENCES

[1] R.S. Wagner, and W.C. Ellis, Appl. Phys. Lett. **4**, 89 (1964).

[2] E.I. Givargizov, J. Cryst. Growth **31** 20 (1975).

[3] A. M. Morales and C. M. Lieber, Science **279**, 208 (1998).

[4] G. F. Zheng, W. Lu, S.Jin, C.M. Lieber, Adv. Mater. **1**6, 1890 (2004).

[5] V. Schmidt, J.V. Wittemann. S. Senz, U. Gosele. Adv. Mater. **21,** 2681 (2009).

[6] L.T. Canham, Appl. Phys. Lett. **57,** 1046 (1990).

[7] M. Hasan, Md.F. Huq, and Z. H. Mahmood, SpringerPlus **2,** 151 (2013).

[8] M.Nolan , S. O'Callaghan , G. Fagas , and J.C. Greer, Nano Lett. **7**, 34 (2007).

[9] F. Sacconi, M.P. Persson, M. Povolotskyi, L. Latessa, A. Pecchia, A. Gagliardi, A. Balint, T. Frqunheim, A.D. Carlo. Electronic and transport properties of silicon nanowires. J Comput Electron. **6,** 329 (2007).

[10] Y. Cui, Z. Zhong, D. Wang, W. Wang, C.M. Lieber. Nano Lett. **3,**149 (2003)

[11] J. Collinge, X. Baie, V. Bayot, E. Grivei. A Silicon on Insulator Quantum Wire. Solid-State Electronics **39,** 49 (1996).

[12] K. S. Yi, K Trivedi, H. Floresca, H. Yuk, W. Hu, and M. Kim. Nano Lett **11** 5465 (2011).

[13] H. Sellier, G.P. Lansbergen, J. Caro, and S. Rogge, Phys. Rev. Lett. **97,** 206805 (2006).

[14] M. Je, S. Han, I. Kim, and H. Shin. Solid State Electronic **44,** 2207 (2000).

[15] S.Bhattacharyya and S. Samui, Appl. Phys. Lett. **84**, 1564 (2004).

[16] S.Bhattacharyya, D. Churochkin and R. Erasmus, Appl. Phys. Lett. **97**,141912 (2010).

[17] T. E. Park, B. C. Min, I. Kim, J. E. Yang, M. H. Jo, J. Chang, and H. J. Choi, Nano Lett. **11,** 4730 (2011).

[18] J. Tang et al., *Nano Lett.* **13,** 4036 (2013).

[19] S. Kumar et al., *Nano Lett.* **13** 5079 (2013).

[20] A.A. Druzhinin, Yu. M. Khoverko, I.P. Ostrovskii, S.I. Nichikalo, A.A. Nikolaeva, L. Konopko, and I. Stich, Physics and Chemistry of Solid State **13**, 269 (2012).

[21] S.M.Sze, Semiconductor Device Physics and Technology 2nd Edition. John Wiley (2002).

[22] S. Cheng et al. *Microsc. Microanal.* **11**, 2 (2005).

[23] J. H. Parker, Jr., D. W. Feldman, and M. Ashkin. Phys. Rev. Lett. **155,** 712 (1967).

[24] M. Cardona and F.H. Pollak. Phys. Rev. Lett. **142,** 530 (1966).

[25] Z. Su, C. Dickinson, Y. Wan, Z. Wang, Y. Wang, J. Sha, and W. Zhou. Cryst. Eng.Comm, **12,** 2793 (2010).

[26] N. Wang, Y. F. Zhang, Y. H. Tang, C. S. Lee, and S. T. Lee, Appl. Phys. Lett. **73,** 3902 (1998).

[27] J.C. Charlier, X. Blaise, and S. Roche. Rev. Mod. Phys. **79,** 677 (2007).

[28] J. C. Licini, D. J. Bishop, M. A. Kastner, and J. Melngailis. Phys. Rev. Lett. **55**, 2987 (1985).

[29] S. Estévez Hernández, M. Akabori, K. Sladek, Ch. Volk, S. Alagha, H. Hardtdegen, M. G. Pala, N. Demarina, D. Grützmacher, and Th. Schäpers. Phys. Rev. B. **82,** 235303 (2010).

[30] S. Alagha, S. Estévez Hernández, C. Blömers, T. Stoica, R. Calarco, Th. Schäpers. J. Appl. Phys. **108,** 113704 (2010).

[31] S. Cho, K. Song , Recent Advances in Polypyrrole. Handbook of Conducting Polymers 3rd Edition (Florida CRC Press, 1998).

[32] J. Park, G. Kim, V. Krstic, B. Kim, S. Lee, S. Roth, M. Burghard, Y. Park. Nanotransport in polyacetylene single fibre: Toward the intrinsic properties. Synthetic Metals **119** 53 (2001).

[33] M. Han, J. Brant, P. Kim, Phys. Rev. Lett.**104,** 056801 (2010).

[34] X. Wu, J.S. Kulkarni, G. Collins, N. Petkov, D. Almecija, J.J. Boland, D. Erts, and J.D. Holmes, Chem. Mater. **20**, 5954 (2008).

[35] N. Singh, A. Agarwal, L. K. Bera, T. Y. Liow, R. Yang, S. C. Rustagi, C. H. Tung, R. Kumar, G. Q. Lo, N. Balasubramanian, and D.-L. Kwong, IEEE Electron Device Lett. **27**, 383 (2006).

[36] K. I. Chen, B. R. Li, and Y. T. Chen, Nano Today **6**, 131 (2011).

[37] F. Vaurette, J.P. Nys, D. Deresmes, B. Grandidier, D. Stiévenard. J. Vac. Sci. Technol. B, **26,** 945 (2008).

[38] B. Wu, A. Heidlelberg, J.J. Boland, Nat. Mater. **4** 525 (2005).

[39] M. Tabib-Azar, R. Wang, S. Sharma, T.I. Kamins, M.S. Islam, R.S. Williams, Appl. Phys. Lett. **87**, 113102 (2005).

[40] A. Heidlelberg, L.T. Ngo, B. Wu, M.A. Phillips, S. Sharma, T.I. Kamins, J.E. Sader, J.J. Boland, Nano Lett. **6**, 1101 (2006).

[41] A. San Paulo, R.T. Howe, R. He, P. Yang, D. Gao, C. Carraro, R Maboudian, Appl. Phys. Lett. **87**, 053111 (2005).

[42] S. Hoffmann, B Moser, J. Michler, S.H. Christiansen, V. Schmidt, S. Senz, P. Werner, U. Gosele, C. Ballif, Nano Lett. **6**, 622 (2006).

[43] S. Datta.Electronic Transport in Mesoscopic Transport, Cambridge University Press (1995).

[44] J. Nygard. *NT05 Tutorial of Electronic Transport.* Sixth International Conference on the Science and Application of *Nanotubes* (2005).

[45] K.H. Cho et al. Appl. Phys. Lett. **92**, 052102 (2008).

[46] F. Maier, T. Meng, and D. Loss, Phys Rev B 90, 155437 (2014).

[47] M. Bockrath, D.Cobden, J. Lu, A. Rinzler, R. Smalley, L.Balents, and P. McEuen, Nature **397**, 598 (1999).

[48] C. Yoon, M. Reghu, D. Moses, A. Heeger, Phys. Rev. B **50,** 8138 (1994).

[49] A. Bachtold, C. Strunk, J. P. Salvetat, J. M. Bonard, L. Forro, T. Nussbaumer, and C. Schonenberger, Nature **397,** 673 (1999).

[50] A. Nikolaeva, D. Gitsu, L. Konopno, M. Gruf, and T. Huber, Phys. Rev. B **77**, 075332 (2008).

[51] A. A. Abrikosov. Europhys. Lett. **49,** 789 (2000).

[52] J. Hu , T. Rosenbaum. Nature Materials **7,** 697 (2008).

[53] F. Patolsky, G. Zheng, and C.M. Lieber, Nature Protocols **1**, 1711 (2006).

[54] I. Park, Z. Li, A.P. Pisano, and R.S. Williams, Nanotechnology **21**, 015501(2010).

[55] X.T. Zhou, J.Q. Hu, C.P. Li, D.D.D. Ma, C.S. Lee, and S.T. Lee, Chem. Phys. Lett. **369**, 220 (2003).

[56] S.C. Singh, H. Zeng, C. Guo, and W. Cai, *Nanomaterials: Processing and Characterization with Lasers*, First Edition. Wiley VCH Verlag(2012).

[57] S. Wieder, The Foundations of Quantum Theory, United Kingdom Edition, Academic Press (London 1973).

[58] N. Fukata, T. Oshima, T. Tsurui, S. Ito, K. Murakami, science and technology of advanced material,**6**, 628-632 (2005).

[59] R. Egerton, Physical Principles of Electron Microscopy. Springer (2005).

[60] C. Lee, D. Kim, and X. Zheng, *Nano Lett*. **10** 5116 (2010).

[61] Z. Xiong and D.J. Miller, Supperlattices and Microstructure **19,** 263 (1995)

[62] F. Rueb, A. P. Micolich, W. Pok, K. E. J. Goh, A. R. Hamilton, and M. Y. Simmons, Appl. Phys. Lett. **92,** 052101 (2008).

[63] Y. Cui, X. Duan, J. Hu, C.M. Lieber, J. Phys. Chem. B, **104**, 5213(2000).

[64] Y. Zheng, C. R. Lake, K. Alam, T.B. Boykin, and G. Klimeck, IEEE Transactions on Electron Devices **52** 1097 (2005).

[65] N. E. Staley, C.P. Puls, and Y. Liu, Phys. Rev. B **77,** 155429 (2008).

[66] D. K. Ferry, S. M. Goodnick, and J. Bird, *Transport in Nanostructures*, Cambridge University Press (2009).

[67] S. Wiedmann, H. J. van Elferen, E. V. Kurganova, M. I. Katsnelson, A. J. M. Giesbers, A. Veligura, B. J. van Wees, R. V. Gorbachev, K. S. Novoselov, J. C. Maan, and U. Zeitler, Phys. Rev. B **84**, 115314 (2011).

[68] T. Kawamura, T. Hatori, Y. Nakamura, N. Aoki, J.P. Bird, and Y. Ochiai, J. Phys. Conference Series **109**, 012018 (2008).

[69] Z. Tan, C. Tan, L. Ma, G.T. Liu , and C.L. Yang, Phys. Rev. B **84,** 115429 (2011).

[70] F. Y. Yang, K. Liu, K. Hong, D. H. Reich, P. C. Searson, C. L. Chien, Y. Leprince-Wang, K. Y. Zhang, and K. Han, Phys. Rev. B **61,** 6631 (2000).

[71] T. Ihn. *Semiconductor nanostructures. Quantum States and Electronic Transport*. Oxford University Press (2010).

[72] A. Bachtold, C. Strunk, J. P. Salvetat, J. M. Bonard, L. Forro, T. Nussbaumer, and C. Schonenberger, Nature **397,** 673 (1999).